Fall 2014

Modeling and optimization of energy storage system for microgrid

Xin Qiu

Department: Electrical and Computer Engineering

MODELING AND OPTIMIZATION OF ENERGY STORAGE SYSTEM FOR MICROGRID

by

XIN QIU

A DISSERTATION

Presented to the Faculty of the Graduate School of the

MISSOURI UNIVERSITY OF SCIENCE AND TECHNOLOGY

in Partial Fulfillment of the Requirements for the Degree

DOCTOR OF PHILOSOPHY

in

ELECTRICAL ENGINEERING

2014

Approved
Dr. Mariesa L. Crow, Advisor
Dr. Jonathan W. Kimball
Dr. Pourya Shamsi
Dr. Mehdi Ferdowsi
Dr. Andrew Curtis Elmore

PUBLICATION DISSERTATION OPTION

This dissertation has been prepared in publication format. Section 1.0, pages 1-16, has been added to supply background information for the remainder of the dissertation. Paper 1, pages 17-45, is entitled "A Field Validated Model of a Vanadium Redox Flow Battery for Microgrids", and is accepted by the *Institute of Electrical and Electronics Engineers (IEEE) Transactions on Smart Grid, Vol. 5, Issue 5, Pages 1592-1601.* Paper 2, pages 46-67, is entitled "A Balance-of-Plant Vanadium Redox Battery System Model", and is prepared in the style used by the *IEEE Transactions on Sustainable Energy* as submitted on August 18, 2014. Paper 3, pages 68-90, is entitled "Heterogeneous Energy Storage Optimization for Microgrids", and is prepared in the style used by the *IEEE Transactions on Smart Grid*, as submitted on October 23, 2014.

ABSTRACT

The vanadium redox flow battery (VRB) is well suited for the applications of microgrid and renewable energy. This thesis will have a practical analysis of the battery itself and its application in microgrid systems.

The first paper analyzes the VRB use in a microgrid system. The first part of the paper develops a reduced order circuit model of the VRB and analyzes its experimental performance efficiency during deployment. The statistical methods and neural network approximation are used to estimate the system parameters. The second part of the paper addresses the implementation issues of the VRB application in a photovoltaic-based microgrid system. A new dc-dc converter was proposed to provide improved charging performance. The paper was published on IEEE Transactions on Smart Grid, Vol. 5, No. 4, July 2014.

The second paper studies VRB use within a microgrid system from a practical perspective. A reduced order circuit model of the VRB is introduced that includes the losses from the balance of plant including system and environmental controls. The proposed model includes the circulation pumps and the HVAC system that regulates the environment of the VRB enclosure. In this paper, the VRB model is extended to include the ESS environmental controls to provide a model that provides a more realistic efficiency profile. The paper was submitted to IEEE Transactions on Sustainable Energy.

Third paper discussed the optimal control strategy when VRB works with other type of battery in a microgird system. The work in first paper is extended. A high level control strategy is developed to coordinate a lead acid battery and a VRB with reinforcement learning. The paper is to be submitted to IEEE Transactions on Smart Grid.

ACKNOWLEDGMENT

I would like to thank Dr. Mariesa L. Crow, my adviser and the chairman of the committee. Without her, the journey of my PhD will not be this rewarding and joyful. Her insights and knowledge are integral to the formation of this dissertation. I would also want to say thank you to Dr Andrew. C. Elmore, who's always been helpful though the on-site work of all my projects.

I want to thank the remainder of my committee, Dr Jonathan W. Kimball, Dr Mehdi Ferdowsi and Dr Pourya Shamsi. I learned a lot of useful knowledge from their classes. Without them, my research will not be finished.

I would thank my parents for their support and encouragement. Their expectation for my academic achievement has always been a good motivation.

At last, I want to express the gratitude to my wife, Chen Wang, who takes care of me with her incessant love and patience. From her, I can always gain the strength and confidence.

TABLE OF CONTENTS

LIST OF ILLUSTRATIONS

LIST OF TABLES

1. INTRODUCTION

According to the US Department of Energy, the smart grid generally refers to the class of technologies being introduced to bring utility electricity delivery systems into the 21st century, using autonomous control [1]. The smart grid concept is often predicated on the widespread evolution of autonomous microgrids. The main envisioned features of the future distributed microgrid system include: automatic controls for electric power at the customer side, a power distribution infrastructure that encourages renewable energy development, local energy storage, and customer loads that are capable of responding to changes in the grid. The smart microgrid offers many benefits to utilities and consumers, mostly seen in improvements in energy efficiency on the electricity grid.

MILITARY forward base camps depend almost entirely on electric power from the local (indigenous) utility or from the camps diesel generators to supply their needs. For tactical installations, this is a significant risk factor as electricity from local utilities may be unreliable and prone to intermittent blackouts, which could compromise critical mission facilities. Diesel generators rely on fuel, which must be transported from storage to the point of use, and may be subject to transportation delays and other competing, mission-critical demands. Integration of renewable energy and advanced energy storage technologies may mitigate the risks and uncertainties of FOB electrical distribution systems. The proposed advanced base camp electrical power system as figure 1.1 will include a distributed microgrid system that incorporates capabilities to monitor and control the operation of distributed resources, including solar, wind, utility grid, diesel, and energy storage units, to dispatch the available resources to meet mission critical loads [2].

Energy storage technology is a critical aspect of future development of portable, scalable microgrid technology. A variety of energy storage technologies have been

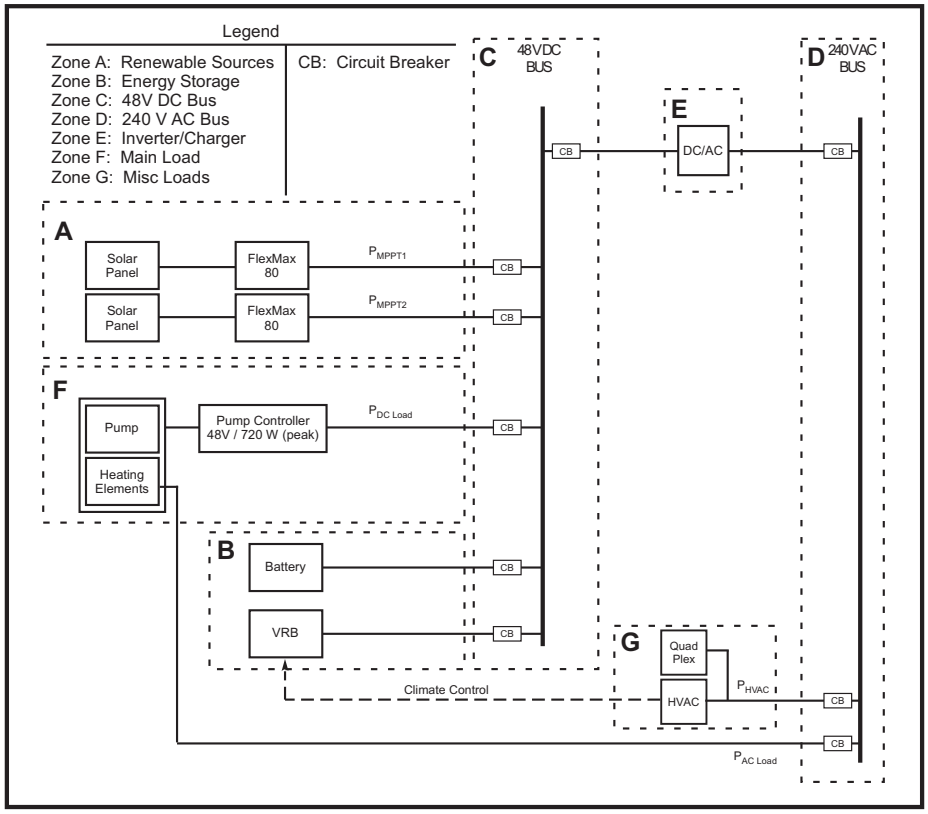

Figure 1.1. Field Microgrid System

extensively reviewed in [4, 5]. The authors discussed the chemical background, manufacturing process, application feasibilies and economical potential etc. Current energy storage technologies such as lead acid batteries contain low energy density at a high mass ratio, require considerable maintenance, and suffer from a limited useful lifetime when deep-cycled on a daily basis [3]. Vanadium redox batteries (VRBs) have recently emerged as a viable energy storage technology due to their high efficiency, high scalability, fast response, long lifetime, and low maintenance requirements. The introduction will talk about basic mechanism of a chemical battery, electrochemistry

and structure of VRB, previous VRB models, a balance-plant view of VRB and heterogeneous energy storage optimization.

1.1. BATTERY ELECTROCHEMICAL PRINCIPLES

A battery is a device that can transform the chemical energy to electrical energy or maybe the reverse way. The electrons are produced from the oxidation and reduction reaction that occurs in the battery. If decomposed to possibly smallest parts but still representative of the battery operation mechanism, it is made up of several so called cells connected in serial or parallel way. The cell is the term more commonly referred to as when the electrochemical aspects of the battery are discussed [6].

Normally a cell can be separated into two half-cells for better analysis. Each cell contains the chemical solution, namely electrolyte and an electrically conductive material immersed in the electrolyte, namely electrode. There is a layer made up of a membrane or a salt bridge, which splits and also intermediates the electrolytes. It does not allow the electrons to pass but can partly or wholly transfer the ions between the two electrolytes in terms of the battery application. The electrodes do not touch each other and only has the electrical connection through the electrolyte. When the chemical reaction starts, species from one half-cell will lose the electrons and another gains them. The party losing the electrons has the oxidization with it and the gaining the reduction. When combined together, the reaction is called reduction-oxidization or simply redox. Moreover, the electrode where the anions (negatively charged ions) go to is the anode or negative electrode and the one where the cations go to is the cathode or positive electrode.

Figure 1.2 illustrates the cell operation during redox reaction. One copper bar and one zinc bar are dipped in the sulfates of the respective metals. The electrolytes are separated by a porous membrane. When the cell is discharging as figure 1.2 (a), the electrons leave the anode that is oxidized and the cathode that is reduced gains the electrons. Direct current is established to supply the load and movement of anions

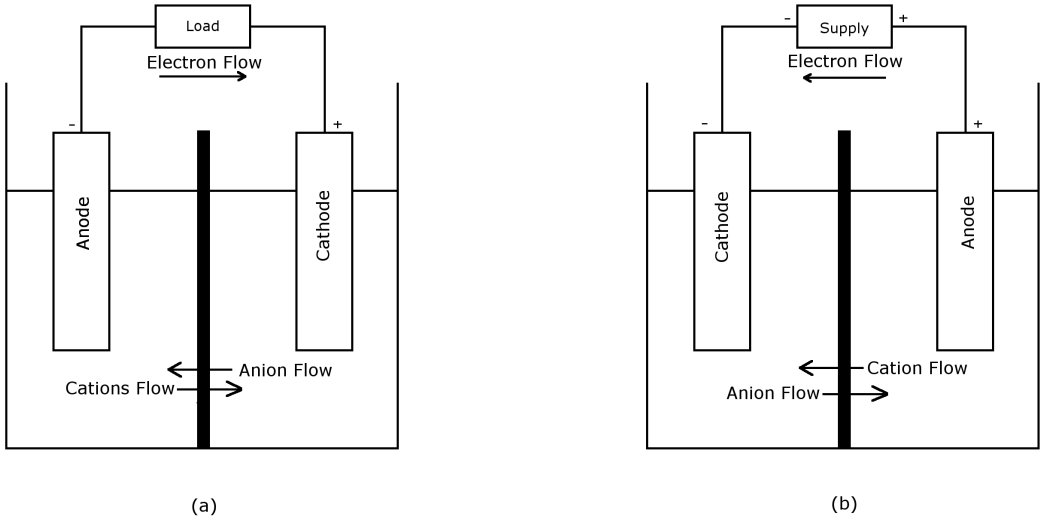

Figure 1.2. Illustration of the Cell Operation

and cations complete the circuit. The reaction at the anode half looks like

$$Zn \rightarrow Zn^{2+} + 2e \tag{1}$$

The reaction at the cathode half is as

$$Cu^{2+} + 2e \rightarrow Cu \tag{2}$$

The overall reaction is

$$Zn + Cu^{2+} \rightarrow Cu + Zn^{2+} \tag{3}$$

When the cell is being charged as Figure 1.2(b), the electron flows in the reversed direction and the positions of anode and cathode are interchanged. The anode becomes the positive electrode and the cathode becomes the negative one.

The reaction at the cathode half is

$$Zn \rightarrow Zn^{2+} + 2e \tag{4}$$

The reaction at the anode half is

$$Cu \rightarrow Cu^{2+} + 2e \tag{5}$$

The total reaction is

$$Zn + Cu^{2+} \rightarrow Cu + Zn^{2+} \tag{6}$$

1.2. VRB ELECTROCHEMISTRY AND STRUCTURE

The chemical reactions occurs in the two VRB cell are as

$$VO_2^+ + 2H^+ + e^- \Leftrightarrow VO^{2+} + H_2O \tag{7}$$

$$V^{2+} \Leftrightarrow V^{3+} + e^- \tag{8}$$

The total reaction is as

$$V^{2+} + VO_2^+ + 2H^+ \Leftrightarrow VO^{2+} + V^{3+} + H_2O \tag{9}$$

The VRB takes advantage of the vanadium ions that can exist in 4 valances so that in each half reaction, vanadium ions only change in valence other than state and the electrode does not take part in the reaction. One good thing about this is that there is no deposit any more. Most of the active species are stored in the external tanks, so electrolytes should be pumped in and out the battery cells continuously.

A vanadium redox battery has more components than a cell encapsulation, but the key part of an VRB is still its cell stack. A cell stack contains several cells compressed together to scale up the output voltage. Each cell has the structure as Figure 1.3, which includes bipolar plate, electrode, ion exchange membrane. Unlike most of the conventional batteries and even redox flow batteries, the electrodes do not participate in the chemical reaction and they are not considered as active species. Usually

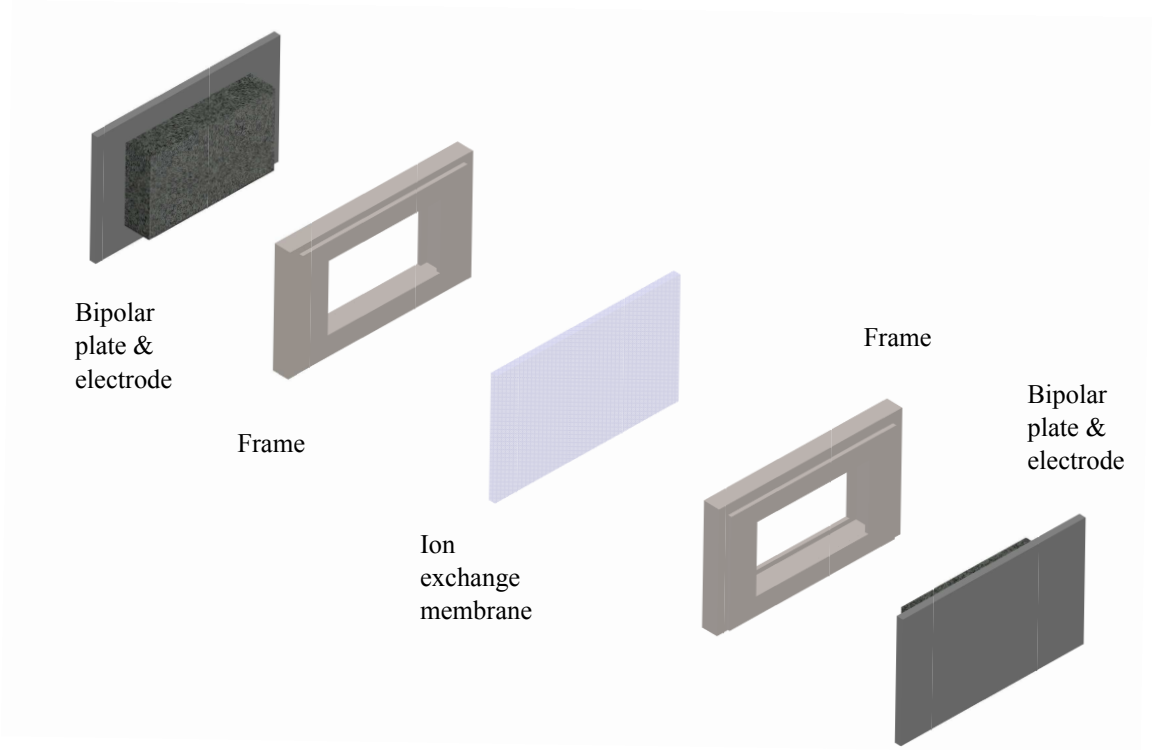

Figure 1.3. Cell Structure

metals like Au, Sn, Ti or nonmetal like carbon make good material for electrodes. Other desirable properties for electrodes include electrochemical reversibility, decent conductivity and a sturdy structure which ease the electrolyte flow and mitigate the polarization. The bipolar plate undertakes the compressive forces to seal the cell and keep the electrodes felt in proper shape. It has winded channels embedded to provide the channel for electrolyte solution and heat exchange fluid. The desired features of a bipolar plate include adequate electrical conductivity, high mechanical performance and strong chemical resistance to the acid solution. Normally, the plate material can be either metal or conductive polymer like carbon-filled composite. Ion exchange membrane is the pivotal part of the cell. It works as the divide between the positive and negative electrolyte while the passage for the proton to move through to sustain the electroneutrality of the electrolyte solutions. Due to its functions, an ion exchange

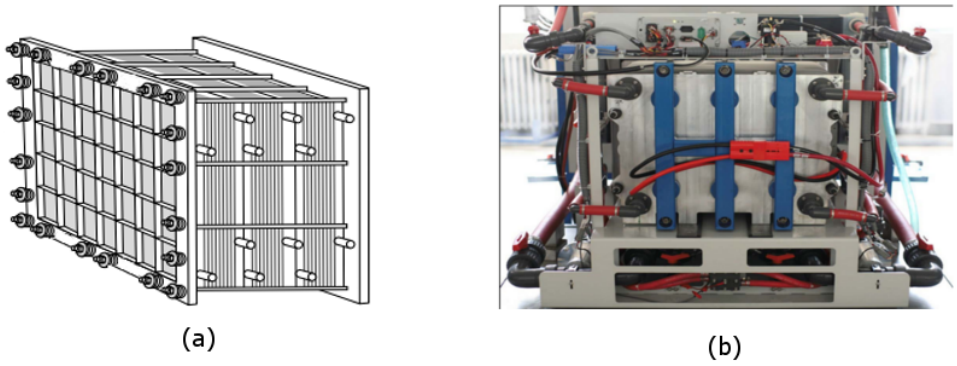

Figure 1.4. VRB Cell Stack Assembly

membrane is expected to inhibit the vanadium from traversing and distinguish proton from other ions and transmit them at higher efficiency. Moreover, it should has sufficient mechanical and chemical strength to resist the corrosion and oxidation [7].

Normally, a single cell would have reduction potential of around 1.5V, which does not fit in most of the power system application. To make the battery practical, multiple cells would be stacked up to push up the voltage and power output. A possible cell assembly implement is shown as Figure 1.4. The bipolar plates, current collectors and end plates are tightened by the bolts and nuts. This kind of structure facilitates the potential further expansion of the stack. Just loosing the bolts and re-tightening them, the room for the new cell would be created. The structure is derived from a common fuel cell stack except for that instead of gaseous reactants, liquid reactants flow through. For a traditional battery, the cell (stack) should be capable of representing the most part of the physical structure and chemical mechanism; it is not the case with the VRB though. The redox flow battery (RFB) needs far more accessories to carry off the energy conversion and transmission. Figure 1.5 shows a commercial VRB process assembly, which includes the stack module, electrolyte solutions, electrolyte tanks, electrolyte circulation pumps, transport pipelines, heat

exchanger, battery controller, AC-DC inverter and other components such as sensors, relays and contactors. The tanks, electrolyte solution, circulation pumps and pipelines constitute the loop of electrolyte recycling. The heat exchange will send out the heat from the reaction from the battery cell. Sensors monitor the system states and send the data to the controller, which can make diagnosis and control decision. The controller also has a serial port as interface for the operators to read the system states. The AC-DC inverter converts the battery DC voltage to AC voltage which can supply the circulation pumps. The pumper driver is also included in the controller.

1.3. PREVIOUS VRB MODELS

VRB is a synergy product of the knowledge from electrochemistry, electricity and mechanics. Each component supports and interacts with each other to make a workable system. A good model should be able to illustrates the process of each

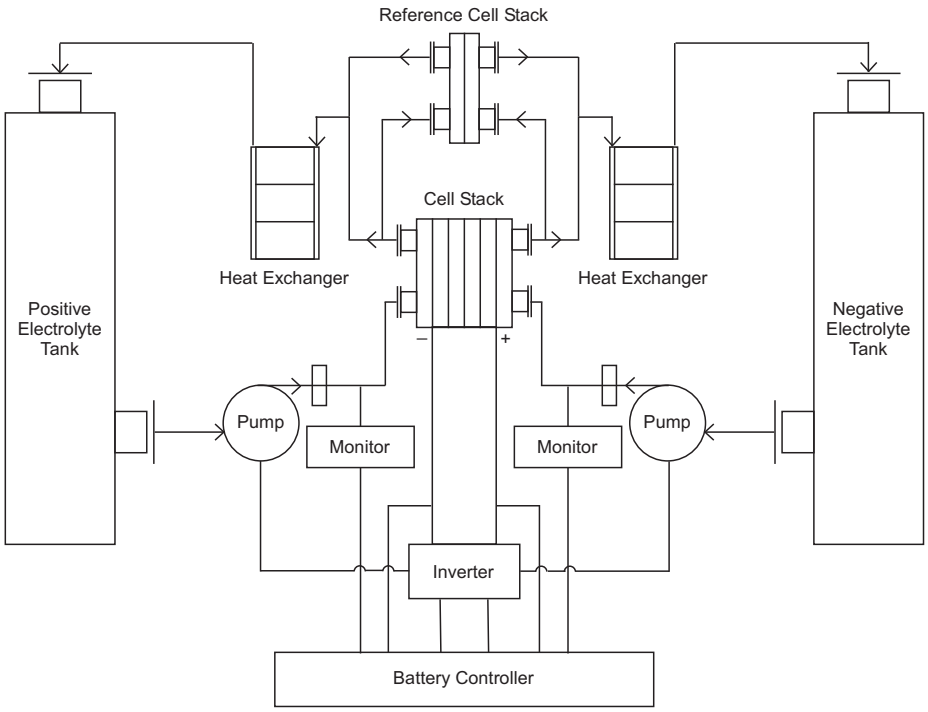

Figure 1.5. VRB Process Assembly

subsystem and also combine all of them to make a complete and conherent system. Cell stack is the core of the VRB, which covered the electrochemical regards. The other important subsystem is the electrolyte delivery, which includes the eletrolyte, the storage tank and the circulation pump. A comprehensive model is proposed in [8], which consists of an electrochemical part handling the cell stack and a mechanical part covering the pipeline and the pump. Various ion concentrations determine the component states. The author went through all the details extensively so that the model is capable of explaining the major aspects of the VRB system.

For the application to the power system, however, the model from [8] does not quite fit in. First, the modeling procedure requires the knowledge of the dimensions and structure of several parts and its analysis with finite element method (FEM). Its not practical for the VRB users to measure the part dimensions. The need for the FEM also weakens the feasibility and universality of the modeling technique. When the VRB is part of a electrical power system, one cares more about its performance on the load leveling capability, the power quality regulation and its efficiency. The model would be more straightforward and compatible with other electrical components if it is converted to an electrical circuit. Chahwan et al offered one simple model which meets the above mentioned expectations [9]. In the model, all the battery elements are converted to electrical circuit components. As shown in Figure 1.6 , a controlled voltage source characterizes the cell stack dynamics and the control input is the state of charge of the VRB. The variety of losses is modeled by resistors and a current source. The cell stack is the place where the reaction happens and therefore the source of the energy. It determines the maximum terminal voltage and the power output. Deemed as a voltage source, the open circuit voltage and thevenin equivalent resistance have to be evaluated.

The open circuit voltage is the electromotive force, which is the equilibrium potential difference of the electrodes when there is no current through the cell. The equilibrium potential is calculated by Nernst equation. As for VRB, at the anode,

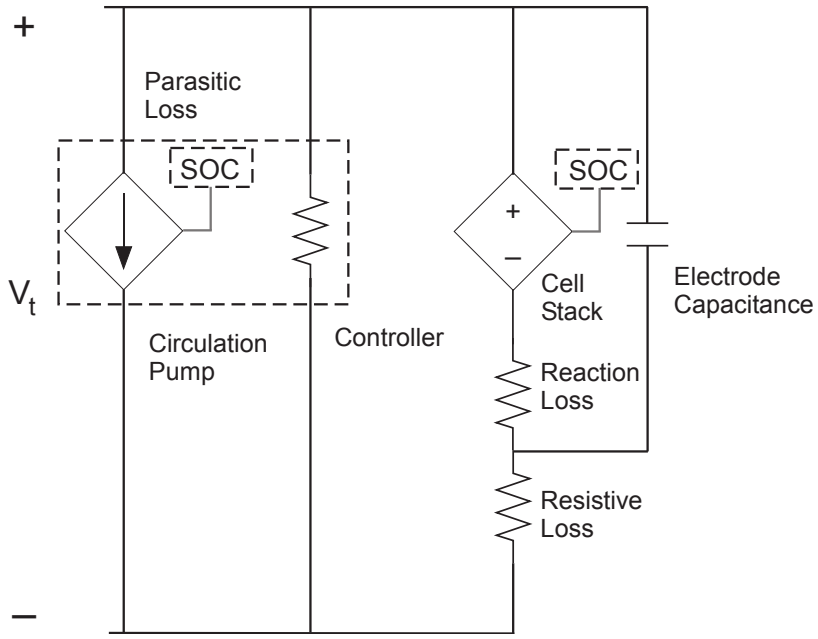

Figure 1.6. VRB Circuit Model Diagram

the equations look like

$$E^{+} = E^{+\prime} + \frac{RT}{nF} ln \frac{C_{VO_2^+} C_{H^+}^2}{C_{VO^{2+}}} \tag{10}$$

At the cathode

$$E^{-} = E^{-\prime} + \frac{RT}{nF} ln \frac{C_{V^{3+}}}{C_{V^{2+}}} \tag{11}$$

The overall electromotive force is

$$E = E^{+} - E^{-} = E_0 + \frac{RT}{nF} ln \left[\frac{C_{VO_2^+} C_{H^+}^2}{C_{VO^{2+}}} \frac{C_{V^{2+}}}{C_{V^{3+}}} \right] \tag{12}$$

(12) where $E^{+\prime}$ and $E^{-\prime}$ are the standard reduction potentials of each half cell, 1.0V and -0.26V respectively. R is the universal gas constant. T is the absolute temperature. n is the transferred electrons per mole of reacting species (n=1 for VRB) and F is Faradays constant [10].

The state of charge (SOC) can be defined as the proportion of low valence vanadium ions to the total, denoted by the concentration, the formula is

$$SOC = \frac{C_{V^{2+}}}{C_{V^{2+}} + C_{V^{3+}}} = \frac{C_{VO_2^+}}{C_{VO_2^+} + C_{VO_2^+}} \tag{13}$$

Take equation (13) to (12), the equation (12) becomes

$$E = E^+ - E^- = E_0 + \frac{RT}{nF} ln \left[\frac{SOC^2 C_{H^+}^2}{(1 - SOC)^2} \right] \tag{14}$$

To eliminate the dependency on the ion concentration, two simplifications are made. First, the proton concentration is neglected, which will cause a little discrepancy between the model and the experiment data [10]. Second, the state of charge is redefined in the practical manner which replaces the concentration with the actual energy. The new SOC formula is as

$$\begin{aligned} SOC_{t+\Delta t} &= SOC_t + \Delta SOC \\ \Delta SOC &= \frac{\Delta E}{E_C} = \frac{P_S \Delta t}{E_C} \end{aligned} \tag{15}$$

where Δt is the simulation time step, P_s is the power output of the cell stack or the voltage source before the impedance, E_c is the total energy capacity of the VRB measured in the unit of . The open circuit voltage now looks like

$$E = E^+ - E^- = E_0 + \frac{RT}{nF} ln \left[\frac{SOC^2}{(1 - SOC)^2} \right] \tag{16}$$

When the VRB runs with the load, the battery terminal voltage diverges from the open circuit voltage. It is caused by a variety of losses. The loss within the stack is denoted by $R_{reaction}$. The one between the stack terminal and the load is denoted by $R_{resistive}$. There is also the parasitic load modeled by the controlled current source. $R_{resistive}$ consists of resistance on the terminal wire and terminal connection. $R_{reaction}$

includes more elements, including activation polarization, concentration polarization and ohmic polarization [6]. The explanations are listed as follows.

- The activation polarization is the extra voltage to initiate and continue the chemical reaction and electron transfer.
- The concentration polarization is due to the concentration difference between the electrode area and the bulk solution.
- The ohmic polarization represents sum of the resistance of the bipolar plates, electrode, ion selective membrane, electrolyte and the active mass in the electrolyte and so on.

Normally, the evaluation of the above mentioned losses relies on the experiment because the mathematical approach is very complex even if the physical parameters of the battery are known.

In [9], the parasitic loss is characterized by a fixed resistance and a current source whose value is calculated by equation (17)

$$I_{pump} = 1.011 \frac{I_{stack}}{SOC} \tag{17}$$

From the experiment, it was observed that the circulation pumps do not operate in the linear way described above. The model also overlooks the fact that VRB has to work optimally under the temperature between $5°C$ to $40°C$. The air-conditioner that might be turned on should also be taken into consideration as part of the parasitic loss. The detailed analysis of the parasitic load is one of the major contributions of this dissertation.

1.4. A BALANCE-OF-PLANT VIEW OF VRB

One of the most important parameters in microgrid operation is the ability to predict the power and energy characteristics of any energy storage system. To achieve

optimal use of renewable energy resources and energy storage, the energy storage system must be modeled accurately. This not only includes modeling of current-voltage characteristics, but must also include all parasitic loads, where the term "parasitic load" refers to the power consumed by the system under no load. The parasitic load includes the power consumption of the ESS balance of plant systems, including the circulation pumps, the heating, ventilation, and air conditioning (HVAC) unit, controllers, and sensors.

In most applications, the VRB is deployed in a standalone enclosure so that the operating temperature can be more closely regulated. Different storage devices have different operating ranges. For example, a valve-regulated lead acid (VRLA) battery has an operating range between 20°C and 45°C, whereas the VRB has an operating range between 5°C and 30°C [11]. Therefore, the environmental modeling and control for these two ESS are quite different.

There is little information in the open literature regarding modeling of ESS enclosure environments. However, there has been numerous studies to predict building energy consumption and these can be extended to enclosure HVAC analysis. Current approaches can be divided into two categories: thermology methods and empirical methods.

The thermology method considers the thermal state variation of each component and their influence upon each other. Partial differential equations or other similar mathematical functions are typically used depending on how precise the modeling is intended. Common inputs to these models include weather conditions, building material and structure, human activity, and the HVAC system.

Empirical methods are used when only a generalized output of the system model is required, such as energy consumption, rather than detailed model characteristics. An empirical method can be used to correlate the desired output to the effective input variables if the intermediate processes are not required. Empirical models based on artificial neural networks (ANN) have been widely researched and applied to energy

consumption related problems [12]. The ANN modeling method is attractive due to its ability to handle model nonlinearities and self-adaption attributes.

In this dissertation, we revise the circuit model of the VRB and present an ANN-based model specifically designed for estimating the parasitic energy consumption of the balance of plant including the enclosure environment and the HVAC. This enhanced model of the VRB energy storage system can be used to better estimate on-site performance when connected to a microgrid.

1.5. HETEROGENEOUS ENERGY STORAGE OPTIMIZATION

The flexible structure and large penetration of distributed energy resources (DER) in microgrids give rise to different operation and control strategies than those of the traditional power systems [13]. Having a diversity of resources in a microgrid is more economic, more secure, and sustainable than relying on a single technology resource; therefore, the future microgrid will most likely rely on a mixture of renewable and nonrenewable types of distributed generation (DG) as well as energy storage. In the future distribution microgrid, multiple types of DG technology and energy storage systems will be connected simultaneously. But coordinating multiple energy storage types can be challenging due to their differences in response times, control mechanics, and charging/discharging efficiencies. The resource variability from the distributed solar PV and wind turbines makes it even harder to manage energy balance. Most research to date has considered only a single energy storage technology at a time and assumes that they operate similarly. However, different types of energy storage technologies have different capabilities, which can be highly beneficial if they are coordinated properly, so that one type of energy storage characteristics complements the others. Due to the combination of renewable energy variation and the uncertainty of local loads, energy storage becomes attractive for maintaining a high and relatively constant load factor and reliable consumer service.

A microgrid with only one energy storage system (ESS) has the advantage of simplicity of control, but may suffer from low efficiency and degradation of lifetime by forcing the ESS to accommodate all power and energy needs. For example, in [14] it was shown that a commercial charge controller designed for lead-acid batteries could not exploit the full potential capability of the deployed VRB, especially at low loads. A microgrid with multiple identical ESS can provide more flexibility, but the individual units may still suffer from many of the same constraints. By introducing multiple types of ESS, a wide range of operating conditions can be met at increased efficiencies. However, heterogeneous ESS suffer from the challenges of incompatible charge controllers, different power/energy versus efficiency characteristics, and different response rates. This result leads to the supposition that the deployment of a variety of ESS could potentially provide better efficiency and reliability if properly interleaved and controlled.

Microgrid control can be divided hierarchically into low level and high level controls. Low level control includes regulating the voltage, current and frequency of the power grid and is typically achieved at the power electronics interface. Higher level controls set the control references for the lower level, based on a variety of considerations such as maintaining an energy reserve, maximizing the overall system efficiency, or optimizing the local power production based on the market price if net metering is presumed.

Most commercially available battery controllers use a form of charge control in which the current input/output of the battery is determined by the bus voltage. In this approach, all batteries connected to the same bus will charge and discharge identically regardless of their individual characteristics. However, to achieve heterogenous control, each ESS must be regulated individually based on a control specific to the capacity, SOC, and type of storage system in use.

Higher level control governs the microgrid power and energy management (PEM). In addition to delivering operational orders to the components, such as synchroniza-

tion in the grid-tied mode or frequency regulation in the stand-alone mode, load-source matching, voltage and frequency regulation, and fault management, the high level control also sets the long term goals and determines the proper operational strategy. The strategies may include minimization of the overall power losses, fuel costs, or power import from the main grid, among others. Due to the different structure and composition from the traditional power grid, microgrid PEM faces other challenges and difficulties [13]. One of the major challenges is the small scale and volatility of the energy resources, which often requires a considerable level of prediction in the optimization process. Off-line optimization such as dynamic programming (DP) can be algorithmically complex and thorough, but suffers from the inaccuracies inherent in predicting behavior. An online optimization can react to new information, but must be computationally efficient to run in real-time. Reinforcement learning (RL) in its simplest form can solve the Markov Decision Process (MDP) problem by DP but has a "learning" part of which DP is incapable. There are several RL applications that have been proposed for power system optimization. For example, [15] implemented a multiple object reinforcement learning method to minimize the fuel cost and enhance the voltage stability at the same time. In [16], a multi agent system was proposed to decrease the power losses of a microgrid, but the battery constraints were not very rigid and allowed uncontrolled charging between the batteries. In this thesis, we propose an interconnection topology and an RL-based algorithm to optimize the coordination of different ESS in a microgrid.

Paper I

A Field Validated Model of a Vanadium Redox Flow Battery for Microgrids

Xin Qiu, Tu A. Nguyen, Joe D. Guggenberger*, M. L. Crow, *IEEE Fellow*, and A. C. Elmore*

Department of Electrical and Computer Engineering

*Department of Geological Engineering

Missouri University of Science and Technology, Rolla, MO 65401

Abstract

The vanadium redox flow battery (VRB) is well-suited for applications with renewable energy devices. This paper presents a practical analysis of the VRB for use in a microgrid system. The first part of the paper develops a reduced order circuit model of the VRB and analyzes its experimental performance efficiency during deployment. The model parameters of the various VRB system components were estimated from experimental field data. The parasitic losses of the circulation pumps power consumption were predicted during different operating situations. The second part of the paper addresses the implementation issues of the VRB application in a photovoltaic-based microgrid system. Commercially available chargers designed for lead-acid battery systems were shown to be non-optimal for VRB systems and a new dc-dc converter control was proposed to provide improved charging performance. The system model was validated with field-obtained experimental data.

Index Terms

microgrid, renewable energy, energy storage, vanadium redox battery, efficiency characterization

I. Introduction

According to the US Department of Energy, the "smart grid" generally refers to the class of technologies being introduced to bring utility electricity delivery systems into the 21st century, using autonomous control [1]. The smart grid concept is often predicated on the widespread evolution of autonomous microgrids. The main envisioned features of the future distributed microgrid system include: automatic controls for electric power at the customer side, a power distribution infrastructure that encourages renewable energy development, local energy storage, and customer loads that are capable of responding to changes in the grid. The smart microgrid offers many benefits to utilities and consumers, mostly seen in improvements in energy efficiency on the electricity grid.

Energy storage technology is a critical aspect of future development of portable, scalable microgrid technology. Current energy storage technologies such as lead acid batteries contain low energy density at a high mass ratio, require considerable maintenance, and suffer from a limited useful lifetime when deep-cycled on a daily basis [2]. Vanadium redox batteries (VRBs) have recently emerged as a viable energy storage technology due to their high efficiency, high scalability, fast response, long lifetime, and low maintenance requirements.

A. VRB characteristics

For a microgrid system, the energy storage system must be capable of high power and long duration. Pumped hydro energy storage (PHES) or compressed air energy storage (CAES) also provide high power and long duration, but they have the drawback of being site-dependent. Li-on batteries are also a promising technology due to high efficiency, energy density, and a low self-discharge rate. However, they are more cost effective for transportation applications and less cost effective for grid-scale applications [3], [4]. VRBs are good candidates to fill the void for high power and energy dense applications due to a number of favorable characteristics inherent to their electrochemical structure:

TABLE I:
Economical characteristics of energy storage system

	PH	CAES	LA	Li-on	VRB
Capital Cost ($/kW)	600-2000	400-800	300-600	1200-4000	500-1500
Capital Cost ($/kWh)	5-100	2-50	200-400	600-2500	175-1000

The VRB differs from traditional battery storage in that the amount of energy it can store is independent of its power rating and is determined by the concentration of the ions in the electrolyte. The size of the VRB stack determines the power rating, whereas the amount of electrolyte determines the energy rating [5], [6]. This power-energy rating decoupling allows for greater flexibility in application and physical footprint. The energy capacity of a fixed stack can be increased "on the fly" by simply adding more electrolyte with limited impact on the footprint and control of the overall system. The power density and energy density of lead acid and Li-ion batteries, by contrast, are not independent and an upgrade in energy capacity requires a complete overhaul of the existing electrical and physical system to accommodate. Furthermore, the VRB can be stored either fully charged or fully discharged for long periods of time without degradation.

A unique feature of the VRB is that the state-of-charge is exactly determined by the amount of electrolyte remaining. This can be directly quantified by measuring the voltage of a reference cell. This ability to accurately track the SOC is a significant advantage over lead-acid or Li-ion batteries in which the SOC is approximated based on voltage levels or tracking historical charge/discharge cycles. The accurate quantification of the VRB SOC enables finer control of energy management which results in a larger range of operation without concern of over-charge or over-discharge resulting in damage to the battery [7], [8].

Flow batteries have a fast response rate due to the speed of the chemical redox reaction in the VRB stack. It typically requires less than 1 ms to track a step change in load, which makes it a an ideal energy storage system to maintain power quality [5].

Some of the first applications of VRBs have been to stabilize wind turbine generator output, by injecting or absorbing active power in antipathy with the turbine output power [9].

The VRB is comparable in cost to several of the energy storage systems currently available. Because of the independent power and energy rating of the VRB, both costs must be considered when comparing various technologies. Table I summarizes typical costs of several energy storage types [10]–[12]. The VRB is a relatively new commercially available energy storage system and it is expected that the costs will decrease in the future as they become more prevalent.

B. Contributions

One of the most important parameters in microgrid operation is the ability to predict the power and energy characteristics of any energy storage system. To achieve optimal use of renewable energy resources and energy storage, the energy storage system must be modeled accurately. This not only includes modeling of current-voltage (IV) characteristics, but must also include all parasitic and power consumption of the HVAC. The term "parasitic load" refers to the power consumed by the system under no load. The parasitic load usually includes the power consumption of the auxiliary systems including the heating, ventilation and air conditioning (HVAC), controllers, and sensors. Furthermore, the energy storage operation must be modeled in conjunction with the particular renewable resource with which it will be used.

Several VRB modeling techniques have been presented in the literature [8], [13]. A physical model is proposed in [13], which consists of both an electrochemical model for the cell stack in which various ion concentrations determine the component states and a mechanical model for the pipeline and the pump. In [8], the VRB system is converted to an equivalent circuit, with the pump treated as a current source and the losses are modeled as resistances. The circuit representation is more computationally efficient and provides reasonable accuracy, therefore we have used the circuit representation as our base VRB model. In this paper, **we further simplify the equivalent circuit, estimate the circuit parameters through measured**

field data, and incorporate an additional component to account for parasitic losses to better estimate round-trip efficiency. The modeling work presented in this paper builds on the modeling efforts presented in [14] in which the VRB efficiency is empirically characterized based on known climatic operating conditions and load requirements. The vanadium redox battery has been advertised as having an 80% efficiency [15], but this figure does not accurately reflect the round-trip efficiency nor does it account for the parasitic losses caused by the circulation pumps and control unit.

Additionally, most commercially available charging systems have been designed for lead acid batteries and when used with other energy storage devices may further adversely affect the efficiency of the system. For this reason, **we propose a new four-quadrant charger and a master-slave control strategy for the charger to improve the VRB efficiency performance**.

II. Microgrid System Description

The microgrid system used to obtain the field data was a standalone system deployed at Fort Leonard Wood, Missouri (latitude 37.71°, longitude 92.15°). The system, shown in Fig. 1, includes a 6 kW photovoltaic (PV) array consisting of 30 × 200 W solar panels (Brightwatts - BI-156-200W-G27V) connected to two Outback FlexMax 80 charge controllers which charged a 5 kW/20 kWhr VRB (Prudent Energy). The system was loaded with two pumps, two condensors, several resistive heating elements, and an HVAC system.

TABLE II:
VRB operating data

Rated power	5 kW
Rated energy	20 kWh
Maximum voltage	56.5 V
Minimum voltage	42 V
Maximum current	140 A
Minimum current	125 A

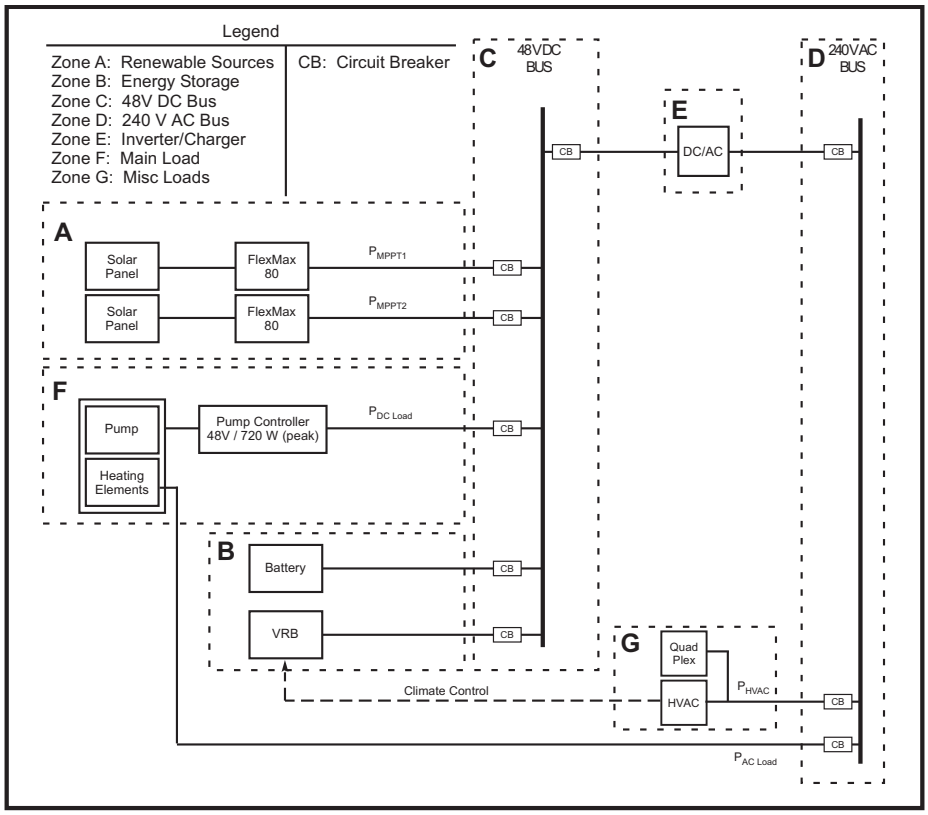

Fig. 1: Field microgrid system illustrating solar panels, loads, and hybrid energy-storage system with battery and VRB

A 38-cell Prudent Energy VRB rated 5 kW/20 kWh is used for energy storage. Table II gives the basic VRB rated operating data. The capacity range of the VRB is specified as 20kWh at a SOC of 73% and 0kWh at a SOC of 20%. It can be charged to a maximum voltage of 56.5 V and discharged to a minimum voltage of 42 V. The VRB energy storage system is self-contained in an enclosure and includes the electrolyte tanks, cell stacks, pumps, and controllers. The enclosure temperature is regulated between 10° C and 30° C via an external heating, ventilation, and air conditioning (HVAC) system.

The system is instrumented to measure environmental data including solar insolation and temperature as well as the voltage and current parameters necessary for monitoring, controlling its operation and characterizing its performance. Operational

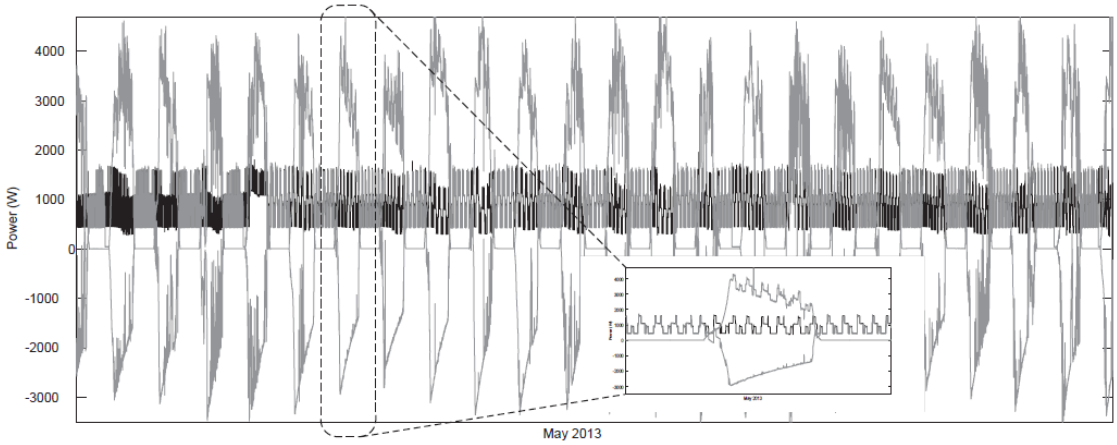

Fig. 2: Microgrid system performance in May 2013 illustrating PV array, VRB, and load powers

data was are recorded using Campbell Scientific Model CR3000 and CR1000 dataloggers which sample every 5 seconds and average the values over a 1 minute window.

The system was designed to be part of a modular military forward operating base (FOB) system that could operate independently, or as part of an integrated system of microgrids. Although the field validation used data obtained from military base operation, it can be generalized to civilian operation since the loads (pumps, compressors, heating elements, and HVAC) are applicable in multiple situations.

The measured performance for the month of May 2013 is shown in Figure 2. The upper trace is the power from the PV array, the lower trace is the power from the VRB (negative indicates charging), and the middle black trace is the load power. During this period, the system is serving a 2 kW (peak) load. A typical day is shown in the inset to provide greater detail. Note that the upper trace, which indicates the power from the PV panel, indicates that the PV power serves both the load (middle trace) and charges the VRB (lower trace). The effects of the two compressors can be clearly seen in the load trace as they switch on and off throughout the day. At night, the power from the PV array goes to zero (indicated by the flat line trace) and the VRB then discharges (becomes positive) to satisfy the load demand. The

data obtained from the microgrid performance will be used to validate the models developed and presented in the following sections.

III. The Vanadium Redox Battery

The vanadium redox battery (VRB) is an electrical energy storage system based on the vanadium-based redox regenerative fuel cell that converts chemical energy into electrical energy. VRBs are a rechargeable battery that consist of an assembly of power cells that requires two electrolytes separated by a proton exchange membrane [7], [16]. A proton exchange membrane separates the solution contained in the power cell where electrolytes are oxidized or reduced. A proton exchange membrane is intended to separate the positive and negative electrolyte solutions while allowing the passage of the charged ions [17]. Without this component, the chemical reaction to transform the energy cannot occur in a meaningful way. The direction of the oxidization reaction determines whether the battery is charging or discharging.

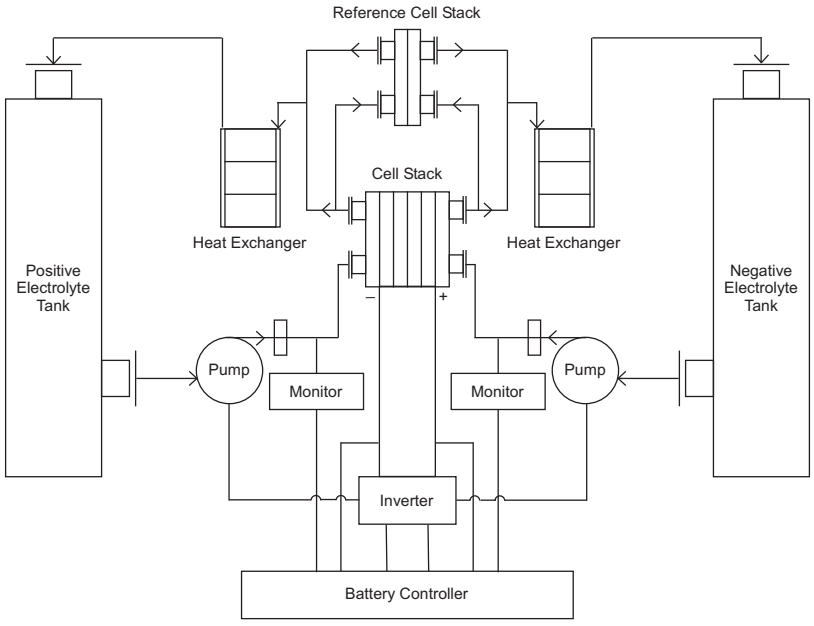

Fig. 3: VRB energy storage system schematic showing physical components

A VRB energy storage system is shown in Fig. 3. The VRB consists of the primary cell stack, two electrolyte tanks (one positive and one negative polarity), two circulation pumps to move the electrolyte through the cell stack, a reference cell stack for monitoring and control, two heat exchangers, instrumentation and control.

The inverter is used to electrically interface the VRB with the external DC system. Several detailed VRB models have been developed to describe the performance of the VRB [8], [13].

Fig. 4 shows the detailed and the proposed simplified electrical circuits for the VRB. Due to the response time exhibited by the dynamics of the PV array and loads, a VRB model on the order of micro-seconds is sufficient. Therefore the electrode capacitor in the detailed model can be neglected and the two resistors can be merged into a single resistor. The parasitic loss block of the detailed model has been replaced with a single controlled current to further simplify analysis. For the simplified model, it is necessary to determine the stack voltage, the equivalent resistance (R_{th}), and the parasitic losses as functions of the state of charge (SOC) and the stack current. The field data collected for analysis include the battery terminal voltage (V_t), terminal current (I_t), the stack voltage (V_s), and the VRB electrolyte pump current (I_p).

Data was collected for a five month period. During the day, the PV arrays supplied the load and any excess energy was used to charge the VRB. During the night, the VRB supplied the load. This VRB performance characterization provides improved accuracy and confidence during the energy management of the microgrid. Furthermore, it allows performance prediction as a function of external environmental features so that the system can be deployed with confidence at various latitudes and longitudes.

Fig. 5 shows the load, PV, and VRB powers over a representative 200 hour (8 day) period during the five month data collection period. Fig. 6 shows the state of charge measured during the same period. Negative VRB power indicates that the VRB is drawing power (charging), thus:

$$\text{PV Power} + \text{VRB Power} = \text{Load Power} \tag{1}$$

A couple of observations can be made regarding the data set. Note that the power from the PV panels is varying significantly during the study period and on day 6 drops significantly. Therefore as the VRB discharges to meet the load, the SOC drops

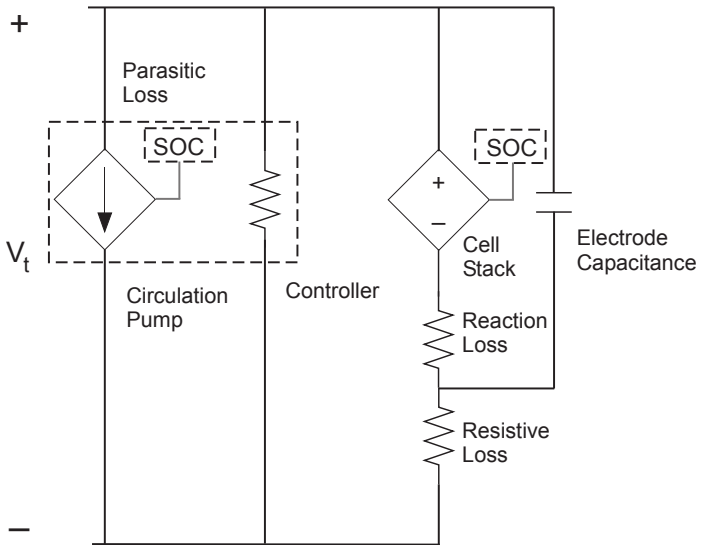

(a) Detailed VRB circuit

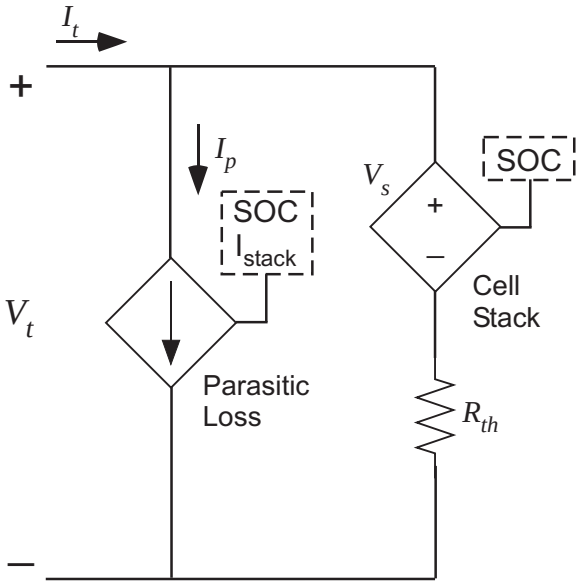

(b) Proposed simplified VRB circuit eliminating electrode capacitance and combined parasitic loss current

Fig. 4: VRB electrical circuits

dramatically as well (Fig. 6). When the SOC drops below 20%, the load is disengaged until there is sufficient PV power available to meet both the load and VRB charging again. The effect of the HVAC (air conditioning) can be seen in the load profile, where the load is higher in the warmer hours of late afternoon.

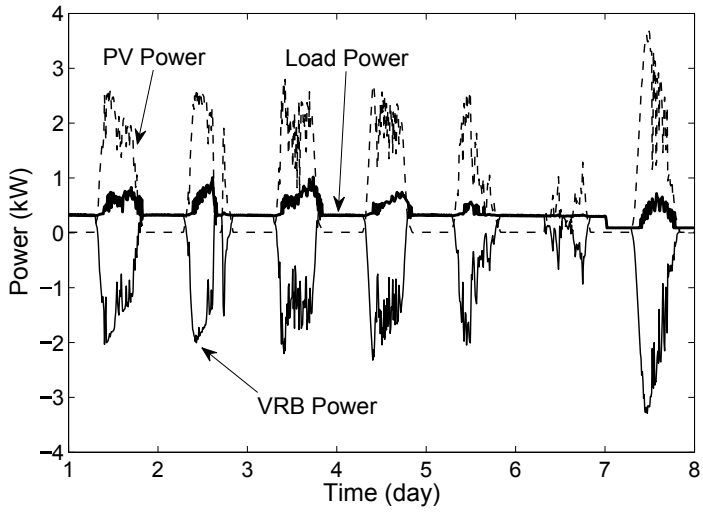

Fig. 5: A Load, PV, and VRB power sample during the data collection period

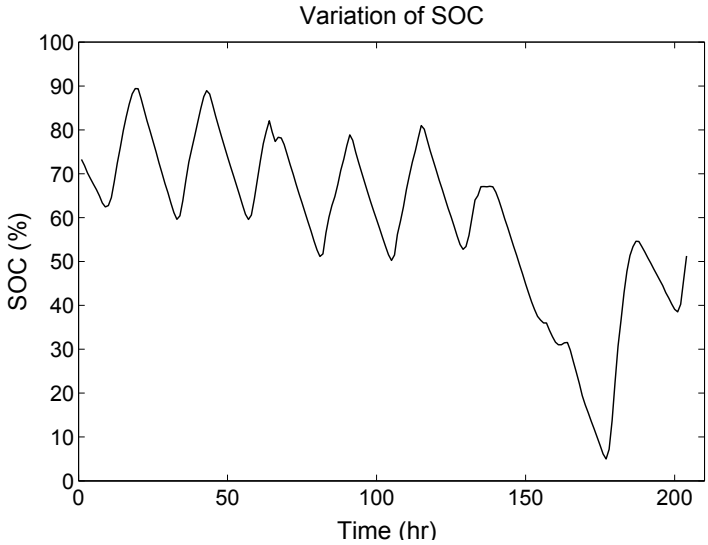

Fig. 6: A State of charge sample during data collection period

IV. VRB modeling and parameter estimation

The data described in the previous section will be used in this section to estimate the parameters of the simplified model of Fig. 4(b).

A. Stack voltage

The open circuit voltage (E) of a single cell can be found from the Nernst equation [13], [18]

$$E = E^0 + \frac{RT}{F} \ln \left(\frac{C_{VO_2^+} (C_{H^+})^2 C_{V^{2+}}}{C_{VO^{2+}} C_{V^{3+}}} \right) \tag{2}$$

where E^0 is the free Gibbs potential, R is the universal gas constant, T is the absolute temperature, F is the Faraday constant and C_X denotes the concentration of the X ions. The concentrations of vanadium ions are

$$C_{V^{2+}} = C_{VO_2^+} = C_V SOC \tag{3}$$

$$C_{V^{3+}} = C_{VO^{2+}} = C_V (1 - SOC) \tag{4}$$

where C_V is the total concentration of all vanadium ions. The stack voltage V_S is E times the number of cells in the stack. The single cell voltage can also be approximated by [19]

$$E = E^0 + \frac{RT}{F} \ln \left(\frac{SOC}{1 - SOC} \right) \tag{5}$$

The SOC varies as the stack power (P_{stack}) changes:

$$SOC_{k+1} = SOC_k + \Delta SOC \tag{6}$$

where the subscript k denotes time interval, and

$$\Delta SOC = \frac{\Delta E}{E_{capacity}} = \frac{P_{stack} \Delta t}{E_{capacity}} \tag{7}$$

where $E_{capacity}$ is the total energy capacity of the VRB. In the model of Fig. 4(b), the ideal current source models the parasitic losses due to the circulation pumps and the controller. The VRB is controlled to remain in a linear operating range between a SOC of 20% and 90% as shown in Fig. 7 [20], therefore (5) can be expressed as

$$E = k_0 + k_1 SOC \tag{8}$$

where k_0 and k_1 can be estimated from the voltage/SOC curve at a given temperature. For example, from the VRB data, when the SOC is in the range of $[0.2 \rightarrow 0.9]$, the linear regression fit for $\ln(\frac{SOC}{1-SOC})$ is $E = 4.75SOC - 2.38$, with an R^2 of 0.99.

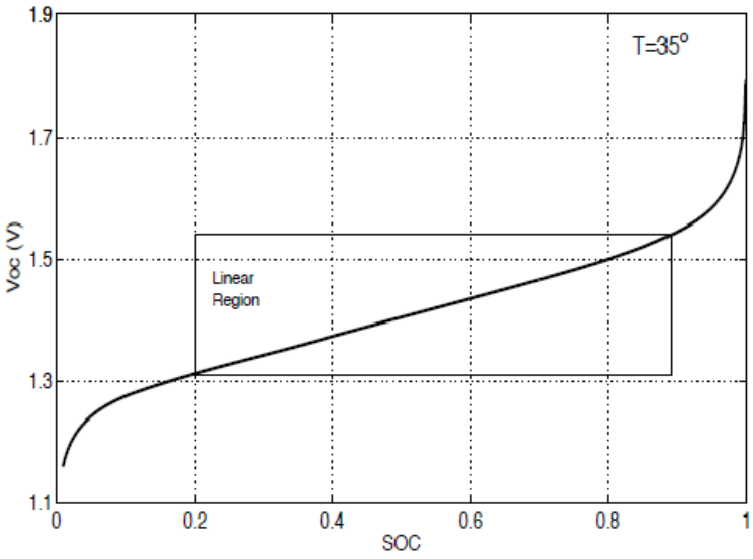

Fig. 7: Open circuit voltage as a function of SOC at $T = 35°C$

B. Equivalent resistance

The instantaneous resistance at any time k can be estimated as

$$R_{th,k} = \frac{V_{t,k} - V_{s,k}}{I_{s,k}} = \frac{V_{t,k} - V_{s,k}}{I_{t,k} - I_{p,k}} \tag{9}$$

where $V_{t,k}$ and $V_{s,k}$ are the terminal and stack voltages at time k respectively, and $I_{s,k}$, $I_{t,k}$, and $I_{p,k}$ are the stack, terminal, and parasitic currents at time k respectively. A general equivalent resistance can be obtained by averaging the instantaneous resistances over the number of measurements N:

$$R_{th} = \frac{1}{N} \sum_{k=1}^{N} R_{th,k} \tag{10}$$

C. Parasitic losses

The VRB is most efficient during heavy operation and its efficiency decreases under low load current. This is due primarily to the parasitic losses caused by the two

electrolyte circulation pumps and the controller. While the controller power draw is relatively constant, the power consumption of the two pumps is directly related to the rate at which the electrolyte is moved through the stack, the pump efficiencies, and the pressure drop [13], [18]. A detailed model of the hydraulic circuit requires finite element analysis, but for electrical efficiency analysis an electrical circuit model is needed. An inverter transforms the DC voltage of the stack to AC to supply the centrifugal pump motor. Fig. 8 shows a motor control loop. If there is a large step

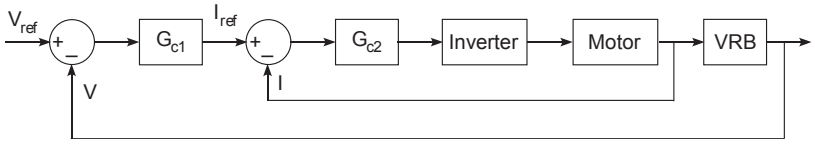

Fig. 8: Pump control loop

change in load, the VRB response depends on the motor pick-up speed and the concentration of the electrolyte. The pump speed is associated with the VRB SOC and in the deployed system, it is a five stage gear pump [14]. Gear staging is a function of both SOC and VRB output power and is consistent during both charge and discharge periods. The parasitic current for the 0-30% SOC region is shown in Fig. 9. The parasitic current has a discontinuous increase at 20A due to a gear change in pump speed. In addition, the parasitic current also has a discontinuous increase at 75A (not shown). We developed a two-layer neural network to perform the function approximation of the parasitic loss. Fig. 10 shows the comparison between the field test data and the estimated parasitic current using the neural network model. The relative similarity of the measured and estimated currents in Fig. 10 validates the neural network approximation and the use of the proposed simplified model. Although the model provides reasonable tracking of the parasitic current, it performs less well in the region immediately preceding a step change in current, such as from 3500 to 4800 minutes. In this region, it is probable that the neural network is over anticipating the step change in parasitic current due to the boundary conditions and reacts too quickly in some cases. The response could be improved by using a more complex neural network structure or a larger training set, but we felt that the results were sufficiently

accurate for our modeling purposes since we are characterizing performance regions and not dynamic responses.

Using the estimated model, the parasitic pump current can be expressed as both a function of SOC and stack current as shown in Fig. 11. The two discontinuities at 20A and 75A are clearly visible. It is also apparent that as the SOC increases, the parasitic pump current increases as well.

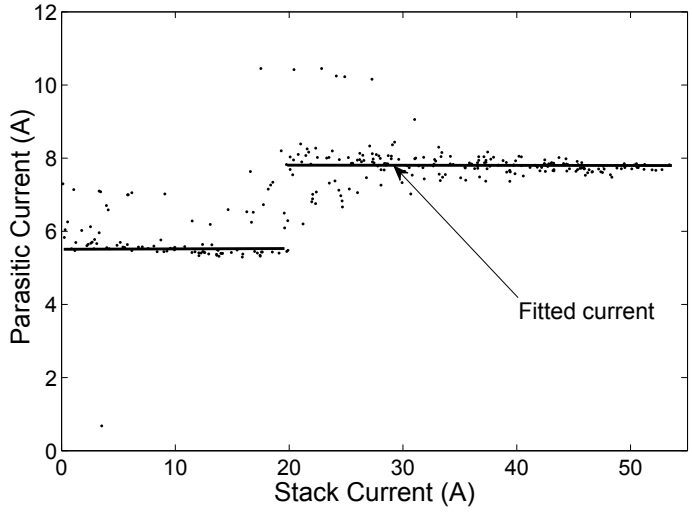

Fig. 9: Parasitic current as a function of stack current (0-30%)

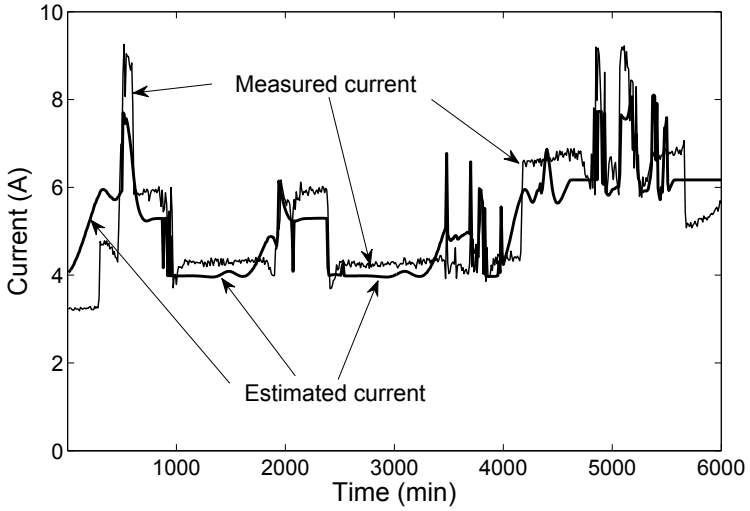

Fig. 10: Parasitic current: measured versus estimated with neural network

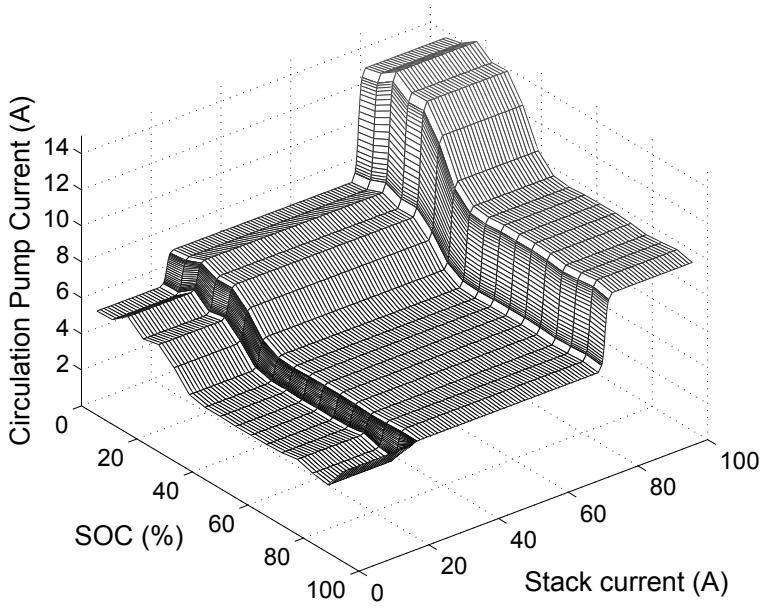

Fig. 11: Parasitic current as a function of SOC and stack current

V. System Efficiency Analysis

In the VRB, the charge and discharge cycles have similar efficiencies [20], therefore only the charging efficiency will be discussed. In the absence of parasitics, the VRB efficiency is dominated by the resistive losses due to R_{th} given in (10) and is therefore nearly linear with the stack current. Without considering the parasitic losses, the SOC has little impact on the efficiency of the system. However, field tests have shown that due to the parasitic losses, the SOC does become an influential factor. Fig. 12 shows the VRB charging efficiency as a function of both SOC and stack current. Note that at low currents, the efficiency decreases dramatically due to the pump current. Once the VRB is engaged, the pump will draw at least 200W regardless of VRB throughput. The VRB is most efficient when loaded at about 75% capacity. This also validates the assertion that the VRB can attain nearly 80% charging efficiency, but not necessarily across all operating conditions.

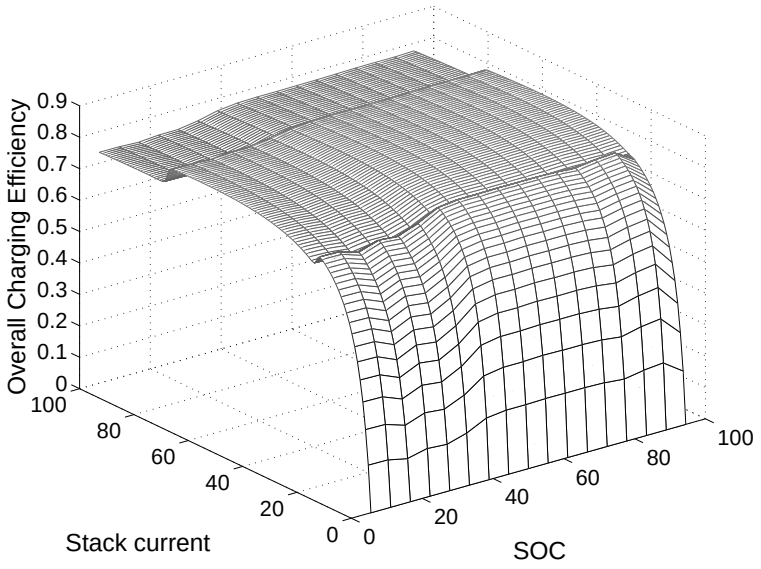

Fig. 12: VRB charging efficiency as a function of stack current and SOC

VI. VRB Operation in Microgrids with Photovoltaics

Unlike lead acid batteries, the VRB has a relatively stable output voltage during charge and discharge. This positive feature actually causes problems in the field when deployed with most (if not all) commercially available inverters and battery charge controllers. In this section, we first discuss the effect of commercial charge controllers on the efficiency of the VRB and then propose a new control strategy suitable for use in microgrids.

A. Charge control

Most charge controllers regulate charging according to a three-stage regime to prevent damage from over-charging. A typical three-stage charging profile is shown in Fig. 13. These stages are:

- Bulk: when the battery voltage is lower than the *absorb* setpoint voltage, the MPPT/charge controller tracks the maximum PV power and charges the battery with the maximum current. The *absorb* voltage level can be set by the user within a pre-defined range.

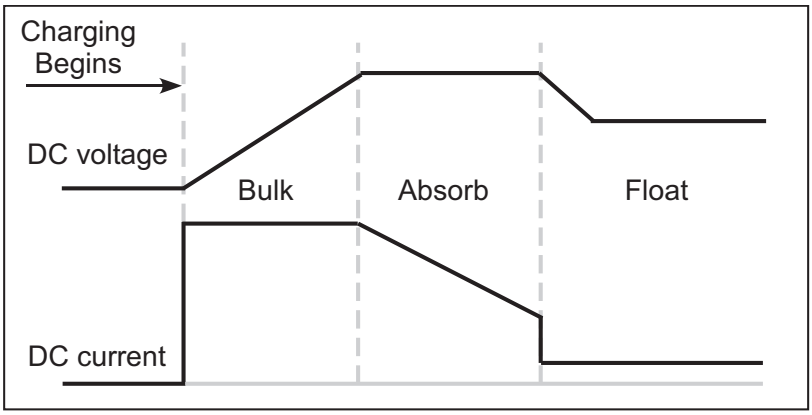

Fig. 13: Typical battery charge regions

- Absorb: when the battery voltage reaches the *absorb* voltage set point, the MPPT/charge controller regulates the battery voltage and charges the battery at a constant voltage.
- Float: when the battery is fully charged, the voltage is decreased and the current is maintained at a small value to account for leakage. This is often known as "trickle charge." A quiescent battery will typically remain in float as long as the battery is connected to the charger.

This charging scheme is used in the vast majority of commercially available charge controllers. The drawback to using this particular charging regime with a VRB is that the lead acid battery voltage set points do not map well to the chemistry of the VRB. With lead acid batteries, the charging current is reduced going from bulk to absorb to protect the battery; however, this is unnecessary with the VRB, which is designed to handle a much higher charging current. The charge controller will prematurely limit the charging current on the VRB. This impact is shown in Fig. 14 which indicates the large region of available PV power which is not being harvested due to the maximum current constraint. Furthermore, if the VRB is set on float (very low current charge) then it will be very inefficient since this is the poorest operating mode of the VRB.

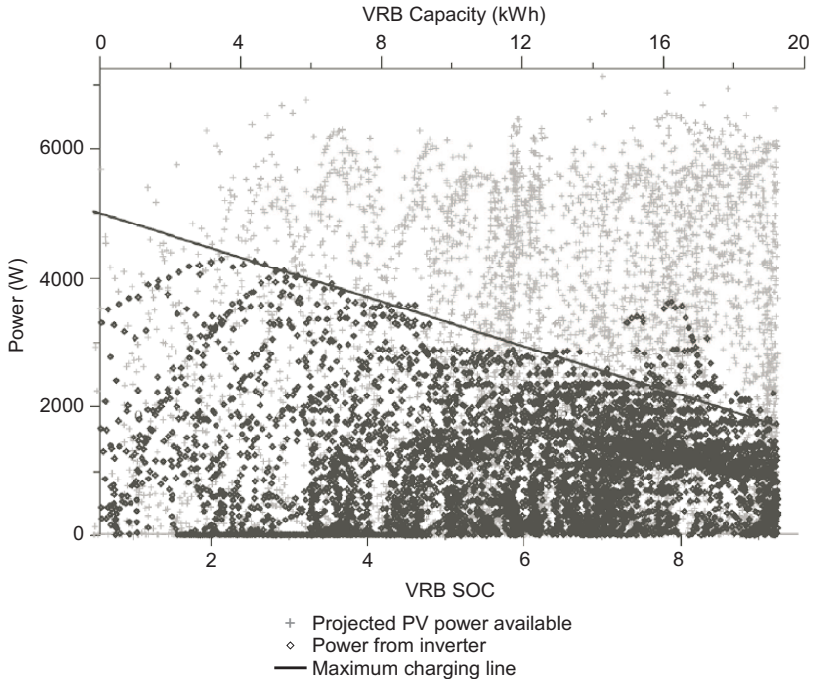

Fig. 14: PV power generation analysis. From [14]

B. Proposed microgrid charge control

Another implementation concern is the low efficiency of the VRB during light load. This concern may be further exascerbated if multiple VRBs are deployed and they jointly share the load, further lowering their individual efficiencies. For this reason, it is important to design charge controllers such that the load is allocated between storage devices in such as way as to maximize the efficiency. To improve the overall system efficiency, we introduce a master-slave control scheme suitable for hybrid energy storage systems to control the power sharing between devices.

Power sharing on a DC bus requires a multi-module parallel converter system. Various converter topologies and their control techniques have been developed for several applications [21]-[25]. However, none of these works specifically implemented organized current sharing to maximize the overall microgrid system efficiency. **We expand on these earlier works to propose both a design and control to maximize the system efficiency**. In our proposed design, the multi-module system is modeled (without loss of generality) as individual converters whose outputs feed

the same DC bus. One of the converters is designated as the master, while the others are the slave units. The master unit regulates the bus voltage and the slave units regulate the current output of their attached storage device. If the master device goes offline (intentionally or unintentionally disconnected), then a new master is elected from among the slave units [26]. An external controller collects information from the solar panels, the load, optimizes the current distribution among the converters, and issues the control settings.

The microgrid system of Fig. 15 is modeled in PSCAD (version 4.3) with two PV panels, a VRB, and a battery is used to illustrate the master-slave control. The battery is modeled as in [27]. Three scenarios are introduced to validate the proposed control: a load change, a power sharing change, and a master-slave exchange.

1) Load Change: In the example shown in Fig. 16, the insolation is relatively constant and both PV arrays output the same power. The load resistance is tuned such that the initial load is 3 kW. The DC bus voltage is 48 V. The VRB is assigned to be the master unit and the battery is the slave. This means that the battery will be assigned to absorb (i.e. charge) 2 kW regardless of load power and the the VRB (as the master) will follow any load changes. This scenario would be suitable for situations in which it is desirable to have the battery charge at a rate which guarantees maximum efficiency of the battery. Note that as the load is reduced from 3 kW to 1 kW, the VRB assumes the entire change in load current as seen in Fig. 16(b) and the battery current remains unchanged. in spite of the current control, there is little effect on the voltages and after a short transient, the DC bus voltage returns to 48V.

At first consideration, this result may seem unremarkable, but this scenario is not possible with current commercially available charge controllers. With most charge controllers, a battery's charge and discharge response are governed solely by the DC bus voltage and cannot be independently commanded. As a result, two batteries in parallel cannot charge and/or discharge independently of each other. With the

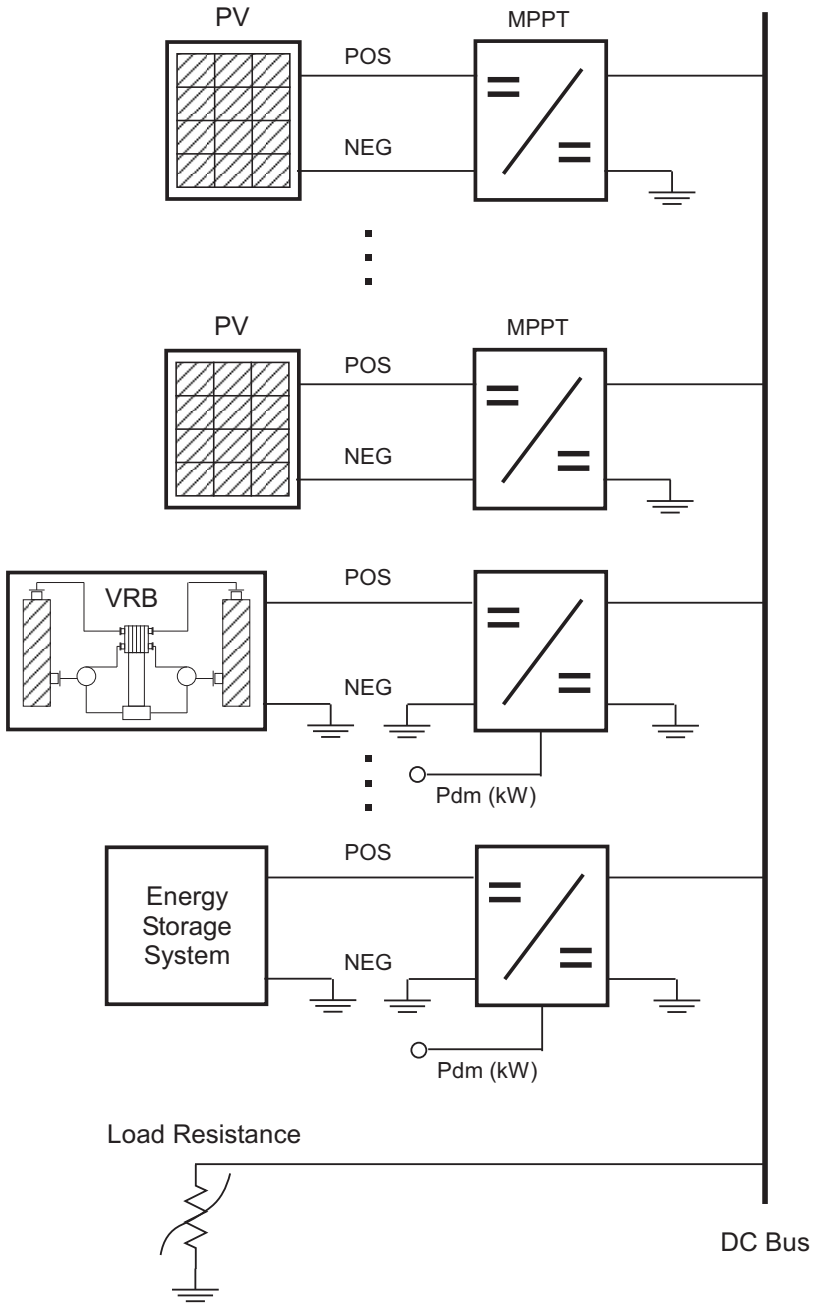

Fig. 15: Microgrid with multiple converter modules

proposed control structure, each energy storage system can be regulated to charge (or discharge) in its most efficient region with only the master performing load following.

2) Change in Power Share: In this example, the PV arrays output the same power as previously, except the load resistance is tuned to absorb 1.5 kW. In this scenario, the battery is the slave and is commanded to absorb 2 kW (charging). At 1.02s, the

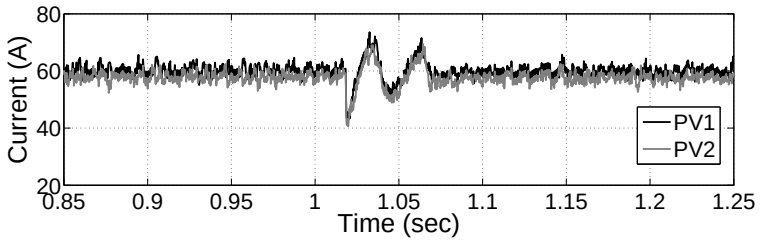

(a) PV currents under constant insolation (constant input power)

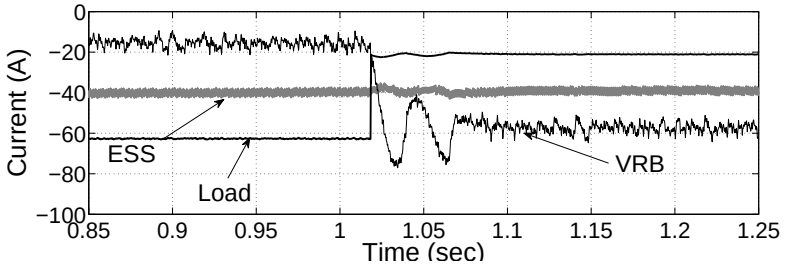

(b) VRB, battery, and load current; the load decreases at 1.02s; the ESS current remains constant; the VRB current assumes the load change

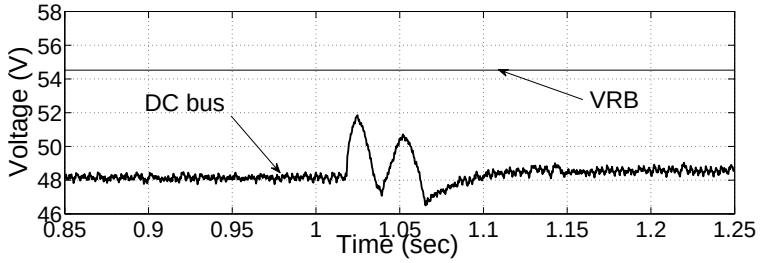

(c) VRB stack and DC bus voltage; the voltages remain relatively constant

Fig. 16: Response to a step change in load

battery is commanded to reduce its charging power to 1kW as shown in Fig. 17. Since the load remains constant at 2kW, the resulting change in power draw is assumed by the master (the VRB). As in the previous example, the DC bus voltage returns quickly to 48 V. This example illustrates the charge/discharge independence of the two energy storage units. Even though the load remains constant, the slave unit can be commanded independently to change its state. This capability is not possible with currently available charge controllers.

3) Master-Slave Exchange: In this example, the PV arrays output the same power as previously and the load is tuned to absorb 1.5 kW. The battery is initially

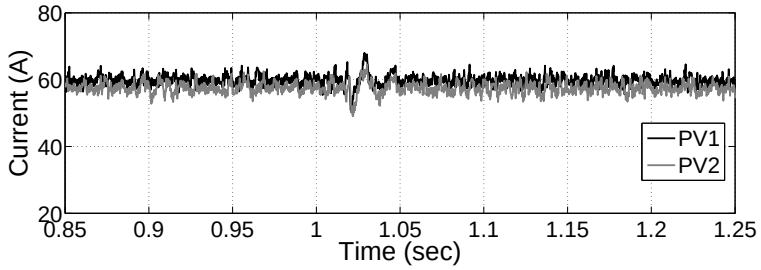

(a) PV currents under constant insolation (constant input power)

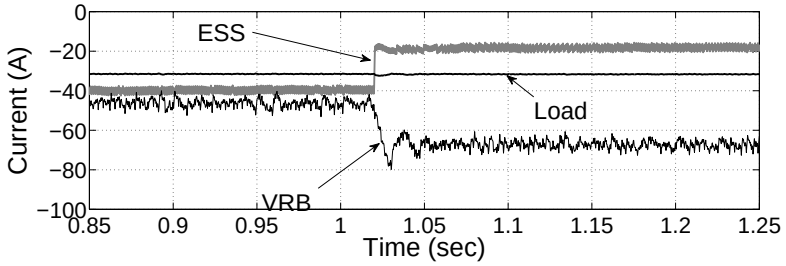

(b) VRB, battery, and load current; the load remains constant; the ESS commanded power is reduced at 1.02s; the VRB picks up the difference

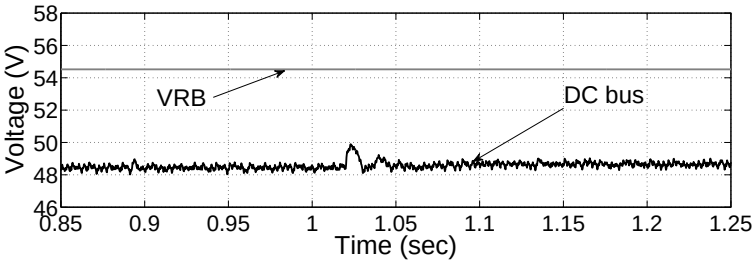

(c) VRB stack and DC bus voltage; the voltages remain relatively constant

Fig. 17: Response to a step change in power share

commanded to absorb 1kW. The master and slave exchange roles such that the VRB becomes the slave unit and the battery is the master. The VRB is commanded to absorb 1kW as the slave unit, therefore the battery (as the master) must assume the load-following role. This example illustrates that the master role is independent of the physical device and that either energy storage device can assume the role as illustrated in Fig. 18. This capability is useful if one of the units either faults or is removed from service; one of the other units in the microgrid can assume the role of the master for seamless operation. This is another capability that it not available with current commercially available charge controllers.

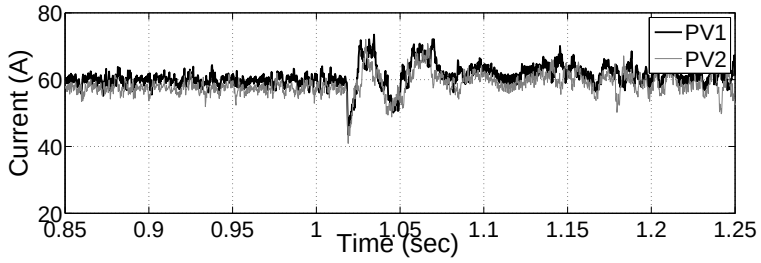

(a) PV currents under constant insolation (constant input power)

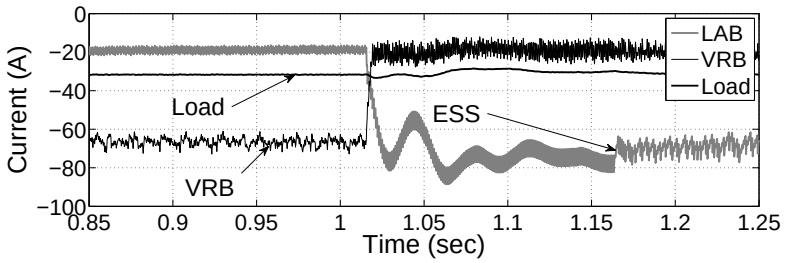

(b) VRB, battery, and load current; at 1.02s the VRB and ESS switch roles; the load remains constant

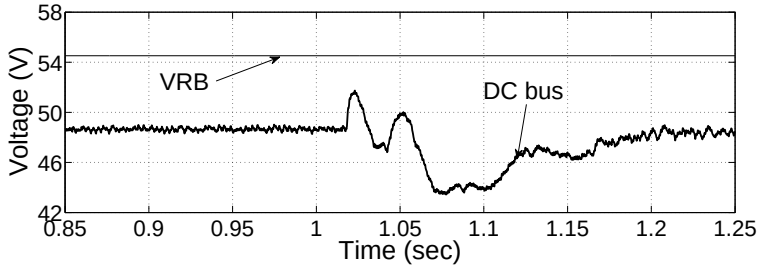

(c) VRB stack and DC bus voltage; the voltages remain relatively constant

Fig. 18: Response to master-slave exchange

VII. Conclusions

This paper outlined three primary contributions:

- A simplified electrical model of the VRB was introduced in which the parasitic pump current was characterized as a function of the VRB state of charge and the stack current. The modeled current was experimentally validated against the measured current. The VRB equivalent resistance was also experimentally obtained.
- The VRB system efficiency was expressed as a function of stack current and VRB state of charge. It was noted that the VRB could attain the near 80% advertised

efficiency over about 50% of the operating range, but drastically dropped for low charging rates.

- It was shown that current commercially available charge controllers typically sold with PV systems are not well-suited for use with VRBs. To counter this effect, a new master-slave control was proposed such that two or more energy storage systems can be used and controlled independently. This functionality is currently not available. This approach was shown to perform as expected through the implementation of three different scenarios.

Acknowledgment

This work has been supported by the Leonard Wood Institute under contract LWI - subaward 400-041

References

[1] Department of Energy, "Smart grid: an introduction." [Online]. Available: http://energy.gov/oe/downloads/smart-grid-introduction

[2] X. Liu and W. Wang, "VRLA battery system reliability and proactive maintenance," in *Telecommunications Energy Conference (INEC), 32nd International*, 2010, pp. 1–7.

[3] K. Divya and J. Ostergaard, "Battery energy storage technology for power systemsan overview," *Electric Power Systems Research*, vol. 79, no. 4, pp. 511–520, April 2009.

[4] H. L. Ferreira, R. Garde, G. Fulli, W. Kling, and J. P. Lopes, "Characterisation of electrical energy storage technologies," *Energy*, vol. 53, pp. 288–298, May 1, 2013.

[5] T. Kaizuka and T. Sasaki, "Evaluation of control maintaining electric power quality by use of rechargeable battery system," in *IEEE Power Engineering Society Winter Meeting, 2001*, vol. 1. IEEE, 28 Jan-1 Feb 2001, pp. 88–93 vol.1.

[6] T. Shigematsu, T. Kumamoto, H. Deguchi, and T. Hara, "Applications of a vanadium redox-flow battery to maintain power quality," in *Transmission and Distribution Conference and Exhibition 2002: Asia Pacific. IEEE/PES*, vol. 2. IEEE, Oct. 2002, pp. 1065– 1070 vol.2.

[7] L. Barote, C. Marinescu, and M. Georgescu, "VRB modeling for storage in stand-alone wind energy systems," in *PowerTech, 2009 IEEE Bucharest*. IEEE, Jul. 2009, pp. 1–6.

[8] J. Chahwan, C. Abbey, and G. Joos, "VRB modelling for the study of output terminal voltages, internal losses and performance," in *Electrical Power Conference, 2007. EPC 2007. IEEE Canada*. IEEE, Oct. 2007, pp. 387–392.

[9] T. Shigematsu, "Redox flow battery for energy storage," *SEI technical review*, no. 73, p. 5, 2011.

[10] H. L. Ferreira, R. Garde, G. Fulli, W. Kling, and J. P. Lopes, "Characterisation of electrical energy storage technologies," *Energy*, vol. 53, no. 1, May 2013.

[11] A. Poullikkas, "A comparative overview of large-scale battery systems for electricity storage," *Renewable and Sustainable Energy Reviews*, vol. 27, pp. 778-788, November 2013.

[12] Petra de Boer and Jillis Raadschelders, "Briefing Paper – Flow Batteries" Jun-2007. [Online]. Available: http://www.leonardo-energy.org/sites/leonardo-energy/files/root/pdf/2007/Briefing

[13] C. Blanc and A. Rufer, "Multiphysics and energetic modeling of a vanadium redox flow battery," in *IEEE International Conference on Sustainable Energy Technologies, 2008. ICSET 2008*. IEEE, Nov. 2008, pp. 696–701.

[14] J. Guggenberger, A. Elmore, J. Tichenor, and M. Crow, "Performance prediction of a vanadium redox battery for use in portable, scalable microgrids," *IEEE Transactions on Smart Grid*, vol. 3, no. 4, pp. 2109–2116, 2012.

[15] "Storage for a sustainable future," Prudent Energy. [Online]. Available: http://www.pdenergy.com/pdfs/Prudent_Energy_Product_Brochure_2011.pdf

[16] L. Barote and C. Marinescu, "A new control method for VRB SOC estimation in stand-alone wind energy systems," in *2009 International Conference on Clean Electrical Power*. IEEE, Jun. 2009, pp. 253–257.

[17] R.-S. Liu, L. Zhang, X. Sun, H. Liu, and J. Zhang, Eds., *Electrochemical Technologies for Energy Storage and Conversion, Volume 1&2*, January 10, 2012.

[18] C. Blanc and A. Rufer, "Modeling of a vanadium redox flow battery," in *PCIM 2007: International Conference on Power Electronics, Intelligent Motion and Power Quality*, 2007.

[19] K. Knehr and E. Kumbur, "Open circuit voltage of vanadium redox flow batteries: Discrepancy between models and experiments," *Electrochemistry Communications*, vol. 13, no. 4, pp. 342 – 345, 2011.

[20] T. Nguyen, X. Qiu. J. Guggenberger, M. L. Crow, and A. C. Elmore, "Performance Characterization for Photovoltaic-Vanadium Redox Battery Microgrid Systems," *IEEE Trans. on Sustainable Energy*, in review.

[21] J. A. A. Qahouq and L. Huang, "Power converter with gradient power architecture and non-uniform current sharing," in *Telecommunications Energy Conference, 2006. INTELEC '06. 28th Annual International*. IEEE, Sep. 2006, pp. 1–8.

[22] P. T. Krein, J. W. Kimball, and B. T. Kuhn, "Non-droop methods for context-sensitive sharing in multi-module switching converters," in *Control and Modeling for Power Electronics, 2008. COMPEL 2008. 11th Workshop on*, 2008, p. 14.

[23] I. Kondratiev, E. Santi, R. Dougal, and G. Veselov, "Synergetic control for m-parallel connected dc-dc buck converters," in *Power Electronics Specialists Conference, 2004. PESC 04. 2004 IEEE 35th Annual*, vol. 1, 2004, p. 182188.

[24] V. Thottuvelil and G. Verghese, "Analysis and control design of paralleled dc/dc converters with current sharing," *IEEE Transactions on Power Electronics*, vol. 13, no. 4, pp. 635–644, July 1998.

[25] P. S. Shenoy and P. T. Krein, "Local control of an isop push-pull converter with uneven load sharing," in *Power and Energy Conference at Illinois (PECI), 2010*. IEEE, 12-13 Feb. 2010, pp. 70–76.

[26] T. Gamage, Y. Liu, T. Nguyen, X. Qiu, B. McMillin, M. L. Crow, and A. C. Elmore, "Intelligent Device Management in Distributed Renewable Energy-based Microgrids," *IEEE Trans. on Smart Grid*, in review.

[27] O. Tremblay and L. Dessaint, "Experimental validation of a battery dynamic model for ev applications," *World Electric Vehicle Journal*, vol. 3, no. 1, 2009, cited By (since 1996): 27.

Xin Qiu received his BS degree of electrical engineering in 2007 from Shanghai Jiaotong University and worked as a design engineer in Cooper Power Systems in Shanghai from 2007 to 2009. He is currently a graduate research assistant at Missouri University of Science and Technology. His research interests are mainly flow battery energy storage systems, renewable energy applications, and microgrid control.

Tu A. Nguyen received his B.S degree in Power Systems from Hanoi University of Science and Technology, Hanoi, Vietnam in 2007. He worked as a Power Transformer Test Engineer in ABB's High Voltage Test Department in Vietnam from 2008 to 2009. He is currently a Ph.D. candidate at Missouri University of Science and Technology. His research interests include microgrid system modeling/analysis and power electronics applications in microgrid systems.

Joe Guggenberger received his B.S. and M.S. degrees in geological engineering from the University of Missouri-Rolla and his Ph.D. degree in geological engineering from the Missouri University of Science & Technology, Rolla. Dr. Guggenberger is employed as an environmental manager specializing in environmental compliance and green engineering. He is a registered professional engineer.

M. L. Crow (S'83–M'90–SM'94–F'10) received the B.S.E. degree from the University of Michigan, Ann Arbor, and the Ph.D. degree from the University of Illinois, Urbana/Champaign. She is the F. Finley Distinguished Professor of Electrical Engineering at the Missouri University of Science & Technology. Her research interests include computational methods for dynamic security assessment and the application of energy storage in bulk power systems.

A. C. Elmore received a B.S. degree in geological engineering from the University of Missouri-Rolla and his M.S. and Ph.D. degrees in civil engineering from the University of Arizona, Tucson. He was employed as a Consulting Engineer with URS Group, Overland Park, KS, where he specialized in green and sustainable environmental remediation. He is currently a Professor of Geological Engineering at the Missouri University of Science & Technology, Rolla.

Paper II

A Balance-of-Plant Vanadium Redox Battery System Model

Xin Qiu, M. L. Crow, *IEEE Fellow*, and A. C. Elmore* Department of Electrical and Computer Engineering

*Department of Geological Engineering

Missouri University of Science and Technology, Rolla, MO 65401

Abstract

The vanadium redox flow battery (VRB) is well-suited for renewable energy applications. It has many attributes which make it an excellent choice for bulk power applications. However, as with all energy storage systems, the energy storage device must consider the balance of plant in computing performance efficiencies. This paper studies VRB use within a microgrid system from a practical perspective. A reduced order circuit model of the VRB is introduced that includes the losses from the balance of plant including system and environmental controls. Experimental field data are collected to estimate the key parameters of the VRB system. The proposed model includes the circulation pumps and the HVAC system that regulates the environment of the VRB enclosure. In this paper, the VRB model is extended to include the ESS environmental controls to provide a model that provides a more realistic efficiency profile.

Index Terms

microgrid, renewable energy, energy storage, vanadium redox battery, efficiency characterization

I. Introduction

According to the US Department of Energy, the "smart grid" generally refers to the class of techniques being introduced to bring utility electricity delivery system into the 21st century using autonomous control. One of the primary objectives of smart grid technologies is to improve the efficiency of the electricity grid [1].

Energy storage is an important part of the future microgrid technology, trending to be more portable, sustainable, and scalable. Conventional batteries such as lead acid units suffer from limited life span, low energy density and high maintenance frequency [2]. As opposed to current storage technologies, flow batteries are receiving more interest due to their high efficiency, high scalability, fast response, long life, and low maintenance requirements. The vanadium redox battery (VRB) is the one of the more recently developed flow batteries. Moreover, the VRB has the advantages of independent power rating and energy capacity, and direct indication of state of charge [3], [4].

One of the most important parameters in microgrid operation is the ability to predict the power and energy characteristics of any energy storage system. To achieve optimal use of renewable energy resources and energy storage, the energy storage system must be modeled accurately. This not only includes modeling of current-voltage characteristics, but must also include all parasitic loads, where the term "parasitic load" refers to the power consumed by the system under no load. The parasitic load includes the power consumption of the ESS balance of plant systems, including the circulation pumps, the heating, ventilation, and air conditioning (HVAC) unit, controllers, and sensors.

Several VRB modeling techniques have been presented in the literature [5], [6]. Reference [5] proposed a physical approach and [6] converts the VRB into a more straightforward equivalent circuit. To study the efficiency performance of a commercial VRB system, [7] developed a circuit model which has more accurate characterization of the circulation pumps. In most applications, the VRB is deployed in a standalone enclosure so that the operating temperature can be more closely regulated. Different

storage devices have different operating ranges. For example, a valve-regulated lead acid (VRLA) battery has an operating range between 20°C and 45°C, whereas the VRB has an operating range between 5°C and 30°C [8]. Therefore, the environmental modeling and control for these two ESS are quite different.

There is little information in the open literature regarding modeling of ESS enclosure environments. However, there has been numerous studies to predict building energy consumption and these can be extended to enclosure HVAC analysis. Current approaches can be divided into two categories: thermology methods and empirical methods. The thermology method considers the thermal state variation of each component and their influence upon each other. Partial differential equations or other similar mathematical functions are typically used depending on how precise the modeling is intended. Common inputs to these models include weather conditions, building material and structure, human activity, and the HVAC system. A typical example is the heat balance method proposed by ASHRAE [9]. This methods focuses on the building components including walls, the interior air, and the heat transfer through including conduction, convection and radiation. The thermology method can give the user a thorough understanding of the system, but it suffers from several disadvantages that limit its extensive application. First of all, it requires large amounts of geometry or material information and considerable expertise to implement. The total thermal process is divided into several solvable subsystems for analysis and for each subsystem, a large number of temperature and heat sensors have to be deployed for data collection. The HVAC itself contains numerous components including a condenser, compressor, accumulator and evaporator, all of which are challenging to model. Furthermore, the model is difficult to calibrate to different operating scenarios (i.e. seasonal changes) [10].

Emperical methods are used when only a generalized output of the system model is required, such as energy consumption, rather than detailed model characteristics. An empirical method can be used to correlate the desired output to the effective input variables if the intermediate processes are not required. Emperical models based on

artificial neural networks (ANN) have been widely researched and applied to energy consumption related problems [11]. The ANN modeling method is attractive due to its ability to handle model nonlinearities and self-adaption attributes. References [12], [13] developed an ANN model to predict heating or cooling loads of a building. The results obtained from the ANN were sufficient to identify the necessary heat gain from the HVAC to maintain the room temperature. This approach is useful for HVAC sizing, but does not provide an accurate indication of the energy consumption of a specific HVAC. An ANN parameterization and training algorithm to forecast long term or short term power consumption was proposed in [14], [15], although the authors' validation tests focused only on large areas or building groups.

In this paper, we revise the circuit model of the VRB and present an ANN-based model specifically designed for estimating the parasitic energy consumption of the balance of plant including the enclosure environment and the HVAC. This enhanced model of the VRB energy storage system can be used to better estimate on-site performance when connected to a microgrid.

II. The Vanadium Redox Battery

The vanadium redox battery (VRB) is an electrical energy storage system based on the vanadium-based redox regenerative fuel cell that converts chemical energy into electrical energy. The VRB is a rechargeable battery that consists of an assembly of power cells that requires two electrolytes separated by a proton exchange membrane. A proton exchange membrane separates the solution contained in the power cell where electrolytes are oxidized or reduced. The proton exchange membrane separates the positive and negative electrolytes while allowing the passage of the ions [16]. The direction of the oxidization determines whether the battery is charging or discharging. A VRB energy storage system is shown in Fig. 1. The VRB consists of the primary cell stack, two electrolyte tanks (one positive polarity and one negative polarity), two circulation pumps to move the electrolyte through the cell stack, a reference cell

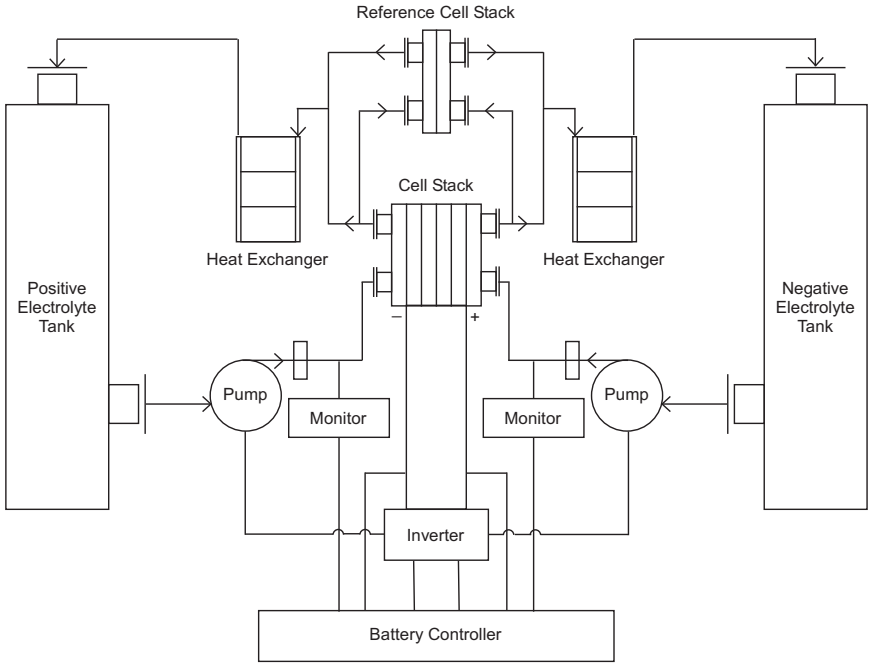

Fig. 1: VRB energy storage system

stack for monitoring and control, two heat exchangers, instrumentation, and control. Several VRB models have been developed [5], [6].

Fig. 2 shows the detailed and the proposed empirical electrical circuits for the VRB. The detailed model captures the electrical behavior of the standalone VRB under ideal environmental conditions [6]. We propose several modifications to this circuit model. Firstly, due to the response time exhibited by the dynamics of the PV array and loads, a VRB model on the order of micro-seconds is sufficient. Therefore the electrode capacitor in the detailed model can be neglected and the two resistors can be merged into a single resistor. One current source represents the parasitic load of circulation pumps and control unit (P&C) and the other current source represents the environmental controls (HVAC). To accurately model the output voltage and current, it is necessary to estimate the stack voltage, the equivalent resistance (R_{th}), and the parasitic losses. The ANN is trained using collected field data that include the battery terminal voltage (V_t), terminal current (I_t), the stack voltage (V_s), HVAC current (I_h) and the VRB electrolyte pump current (I_p).

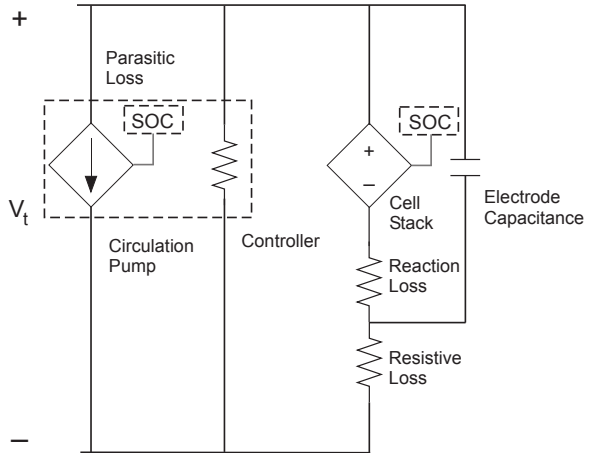

(a) Detailed VRB circuit

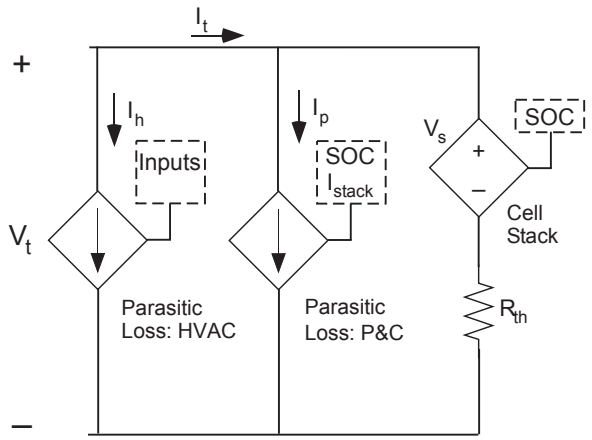

(b) Proposed VRB circuit

Fig. 2: VRB electrical circuits

III. Microgrid system description

The microgrid system used to obtain the field data was a standalone system deployed at Fort Leonard Wood, Missouri (latitude 37.71°, longitude 92.15°). The system, shown in Fig. 3, includes a 6 kW photovoltaic (PV) array (Brightwatts - BI-156-200W-G27V) connected in two parallel strings through maximum power point charge controllers (Outback FlexMax 80) to charge a 5 kW/20 kWhr VRB (Prudent Energy). The PV array and VRB are connected through circuit breakers to a 48 VDC bus. The 48 VDC bus is connected through an inverter to a 240 VAC bus. The enclosure environmental controls draw their power from the AC bus and not from the VRB directly. The system served various loads, including pumps and heating elements

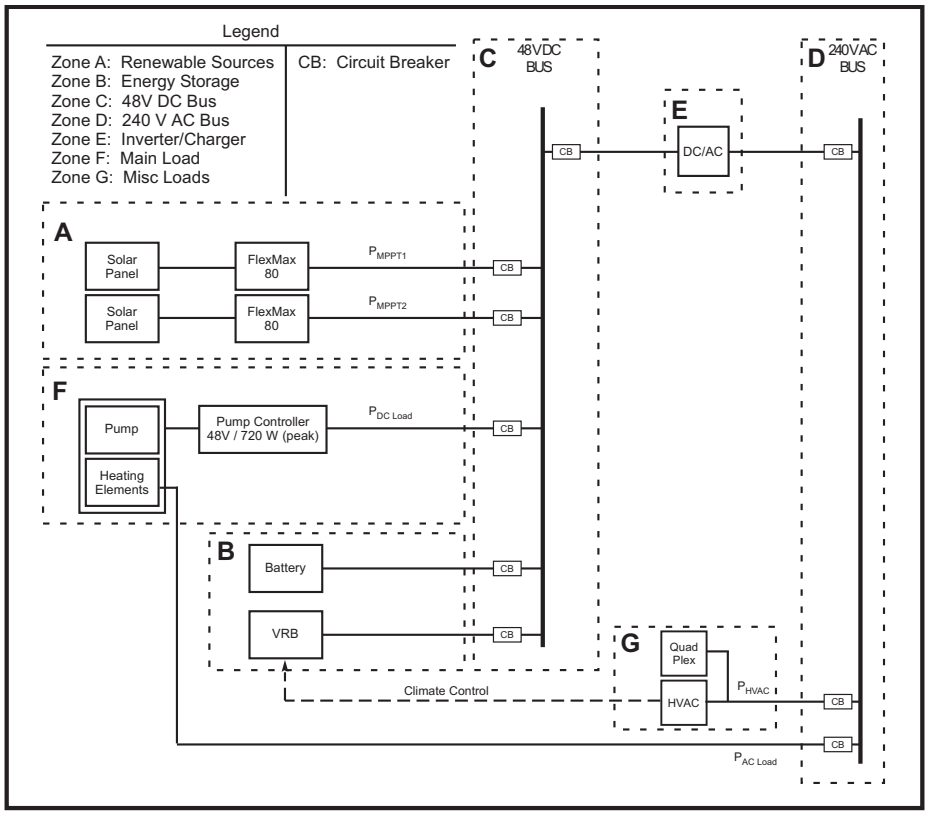

Fig. 3: Field Microgrid System

on both the AC and DC buses to emulate actual operational load behavior. The system was designed to be part of a modular military forward operating base system that could operate independently, or as part of an integrated system of microgrids. Although the field validation used data obtained from military base operation, it can be generalized to civilian operation since the loads are typical of multiple situations. Table I provides the VRB ratings. The VRB energy storage system is self-contained in an enclosure and includes the electrolyte tanks, cell stacks, pumps, and controllers.

The system is instrumented to measure environmental data including solar insolation and temperature as well as the voltage and current parameters necessary for monitoring, controlling its operation and characterizing its performance. Operational data was collected from June 2011 through October 2011. Data was collected every 5 seconds and averaged over a 1 minute window throughout operation. A seven day sample of data is shown in Fig. 4. During the day, the PV arrays supplied the load

TABLE I:
VRB operating data

Rated power	5 kW
Rated energy	20 kWh
Maximum voltage	57 V
Minimum voltage	42 V
Maximum current	140 A
Minimum current	125 A

and any excess energy was used to charge the VRB. During the night, the VRB supplied the load. When the VRB power is negative, this indicates that the VRB is charging (absorbing power), thus:

$$\text{PV Power} + \text{VRB Power} = \text{Load Power} \tag{1}$$

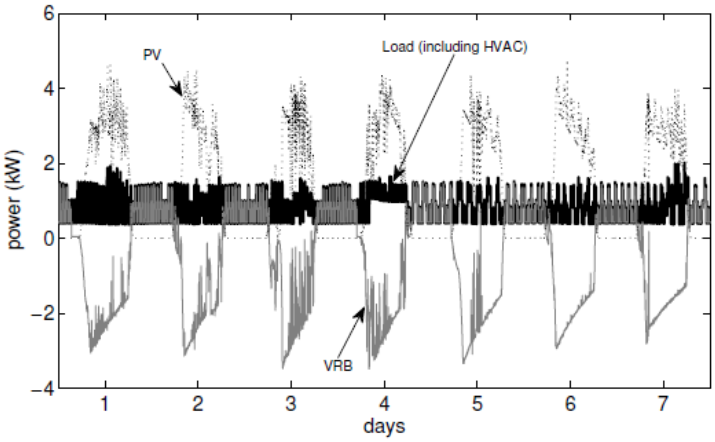

Fig. 4: Load (black line), PV (dashed line), and VRB (grey line) power during data collection period

IV. Enclosure and HVAC

Environmental controls are required for the VRB energy storage system to operate properly. Freezing temperatures can hinder electrolyte flow, whereas high temperatures can damage the VRB membrane, cause the V_2O_5 to precipitate, and cause overheating of the electrical equipment [16]. In this system, the VRB enclosure

temperature is regulated between $10°C$ and $30°C$ by a built-in HVAC system that includes a cooling-heating air conditioner and ventilation fans. The temperature control scheme is:

- Heating is ON when the enclosure temperature is lower than $10°C$.
- Fans are ON when the enclosure temperature is between $25°C$ and $30°C$.
- Cooling is ON when the enclosure temperature is greater than $30°C$.

To better estimate the behavior of the HVAC, the thermal characteristics of the enclosure must first be developed. Although an ANN-based model will ultimately be developed, it is illustrative to first consider the fundamental principles of the physical model of the system to better understand the impact of various parameters.

A. Heat transfer and heat balance of the enclosure

Fig. 5 shows the VRB enclosure from the field microgrid system. The enclosure was provided by the manufacturer. The enclosure is augmented with additional insulation and insolation shielding to better regulate internal temperatures. The enclosure specifications are given in Table II.

Fig. 5: VRB enclosure

Fig. 6 shows the thermal elements involved in the heat balancing process of the enclosure. There are three influences on the heat transfer of the external surface of the

TABLE II:
VRB enclosure parameters

Exterior dimension	3.92m×2.23m×2.36m
Interior dimension	3.80m×2.10m×2.20m
Weight excluding VRB	1900kg
Weight including VRB	6300kg
Exterior cover	0.8mm thick aluminum sheeting
Interior cover	0.8mm thick aluminum sheeting
Inner insulation layer	50mm expanded polystyrene

enclosure: absorbed insolation, convection to outside air, and long wave (i.e. infrared) radiation.

1) Absorbed Insolation: The insolation absorption depends on the solar flux that impinges on the enclosure and the absorptivity rate of the enclosure surface. The incident solar flux is composed of the direct-beam radiation, which is traveling in a straight line from the sun, the diffuse radiation, which is solar energy scattered by the molecules and suspensoids in the atmosphere, and the reflected radiation, which is reflected from the surrounding surfaces [19]. After the location and geometry of the enclosure is known, it is not difficult to calculate the clear sky solar insolation, but the clear sky solar insolation does not include any weather effects. To address the impact of the actual weather, the actual insolation is measured by a pyranometer in the field and will be used as the reference for further calculations. Any shading of the enclosure from the surroundings will also be included. Therefore the actual solar radiation that strikes the enclosure will be used as an input to the ANN model. The absorptivity of the surface is hard to estimate but remains relatively constant, so it will be an internal parameter of the ANN model rather than explicitly quantified.

2) Convection: Convection is one mode of heat transfer, caused by the random motion of the air. Forced convection is air movement caused by an external influence such as the wind or a fan. Natural convection is air movement caused by inherent factors, such as buoyancy. In most applications, both forced and natural convection happen simultaneously in varied proportions [19]. The heat transfer rate by convec-

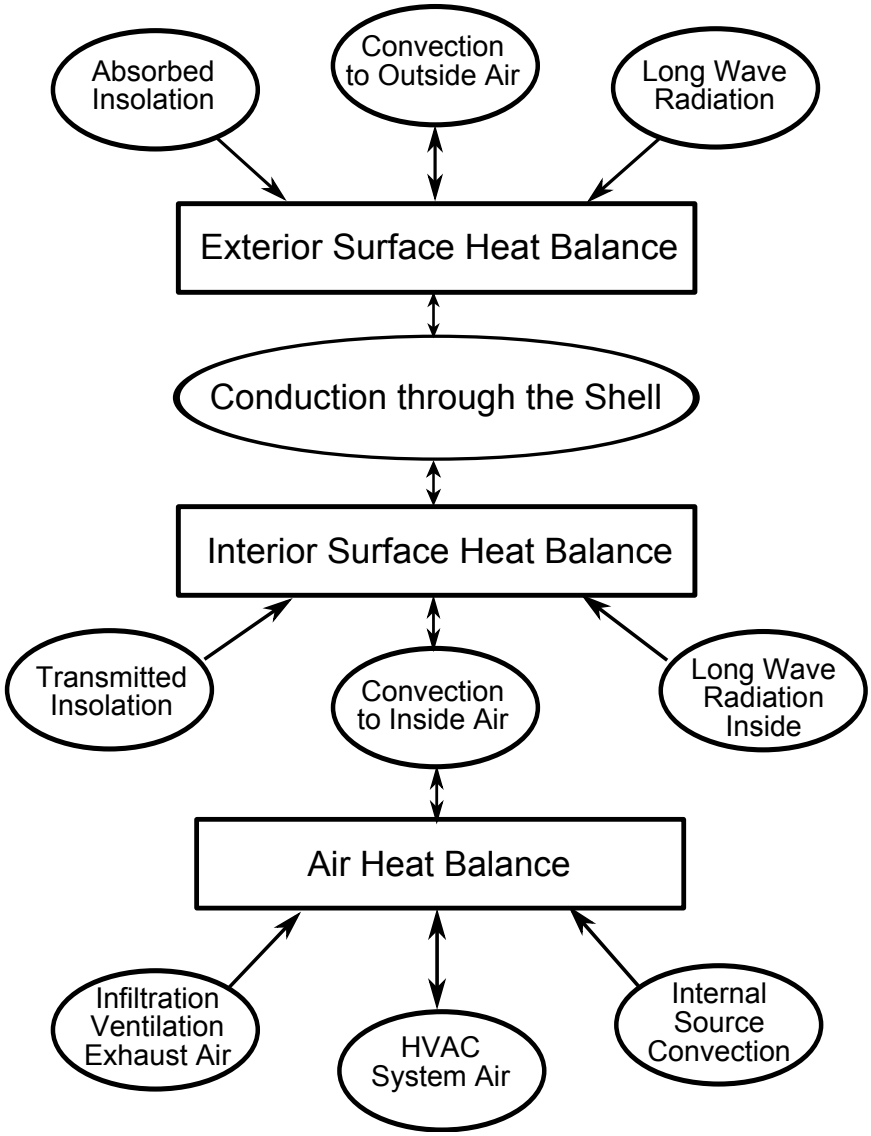

Fig. 6: Heat balance in VRB enclosure

tion is given by

$$\frac{dQ_{conv}}{dt} = hA_s(T_s - T_\infty) \tag{2}$$

where h is the convection heat transfer coefficient ($\mathrm{W°C/m^2}$), A_s is the heat transfer surface area ($\mathrm{m^2}$), T_s is the temperature of the surface (°C), and T_∞ is the temperature of the air sufficiently far from the surface (°C).

Eq. (2) is deceptively simple. In practice, each of the coefficients are multivalued functions of external parameters. The transfer coefficient h depends on a variety of

TABLE III:
HVAC parameters

Model	KFR-35GW/E1(DBP)
Horsepower	1.5
Cooling capacity	3500W
Cooling power	1100W
Heating capacity	4500W
Heating power	1400W

variables including the air fluidity properties and surface roughness and geometry. If the enclosure resides in a turbulent air environment, it will be extremely difficult to estimate this parameter. For buildings, the usual approach is to correlate the coefficients to the wind speed at the target location by experiment or numerical simulation [20]. It is therefore reasonable to use the ambient temperatures and wind properties as inputs to the ANN process to predict the correlations.

3) Long wave radiation: The long wave radiation is the radiation which governs the heat exchange among terrestrial objects such as the earth and buildings [19]. The net radiation exchange on a surface can be described by

$$E = \varepsilon_{sr}\sigma T_{sr}^4 - \varepsilon_s \sigma T_s^4 \tag{3}$$

where ε_{sr} is the emissivity coefficient of the surroundings and ε_s denotes the surface emissivity. The constant σ is the Stefan-Boltzmann's constant and T is the absolute temperature. The thermal dynamics of the enclosure shell and the inside air will be incorporated into the ANN model. There are, however, several elements need to be considered separately.

Sensible heat gain indicates how much heat the HVAC has to remove to maintain the target temperature, thus adding to the parasitic load. The HVAC specifications are given in Table III. The inside air temperature and humidity both play parts in the sensible heat gain q_s such that:

$$q_s = 1.2(1.006 + 1.84W)Q_s\Delta T \tag{4}$$

where 1.006 (kJ/(kg $\cdot$ K)) is the specific heat of dry air, W is the humidity ratio, 1.84 (kJ/(kg $\cdot$ K)) is the specific heat of water vapor, ΔT is the temperature difference, and Q_s is the air flow [9].

Additionally, the internal source convection can be caused by the heat emitted by VRB itself and other devices, such as the controllers and sensors. The heat is roughly proportional to the load of the microgrid system, therefore the load demand may be an adequate input parameter.

B. Input variable selection

The previous section outlined the primary physical characteristics that may have an impact on the VRB efficiency and power output. These identified parameters will be used as initial candidates in constructing the input set to the ANN model. However, not all of the parameters may have significant influence on the output and their inclusion may serve to add to the computational burden. For example, for a multilayer perceptron (MLP), the dimension of the internal ANN weighting matrix is affected by the size of the input, therefore during each training round a large number of matrix elements are calculated and updated. The size of the training data is required to increase exponentially with the model dimensionality to maintain enough confidence [22].

Furthermore, if any of the parameters are redundant (they affect the output in a similar qualitative manner), then combinations of these parameters may lead to convergence to a local optimum [21] as opposed to the desired global optimum. Therefore for these reasons, it is prudent to conduct a sensitivity analysis to determine which of the parameters have the largest influence and neglect those parameters with marginal influence. Therefore, we attempt to rank the elements of the input set in terms of their influence on the desired output.

Influence is determined by the relevance and independence of the elements of the input set. An input can be relevant to the model output, but its independence diminishes if it highly correlates with other input, thus making it less useful. In [23], the "minimal-redundancy-maximal-relevance" (mRMR) criterion is proposed

to quantitatively weigh the importance of the variables. The mRMR index used here is defined as the difference between a relevance term and a redundancy term:

$$\text{mRMR}_i = d(i,t) - \frac{1}{n}\sum_{j\in S} d(i,j), \quad i \in \Omega_S \tag{5}$$

The first term, $d(i,t)$, measures the parameter relevance, which is the distance correlation between the i^{th} input and the target t where i is in the entire set of parameters Ω but not in S, which is the set of already selected inputs. The second term measures the redundancy and is the average of the distance correlation between the i^{th} and the j^{th} input in set S.

Using the min-max criterion, the set of possible input parameters can be searched and selected in an incremental manner. For example, if the input set S has n parameters, then the $(n+1)^{st}$ input parameter added to the set must have the highest mRMR.

The input candidates and their denotation are listed in Table IV. To remove the circular discontinuity, the hour of the day hr is transformed to $\cos(\frac{\pi}{12}hr)$ and $\sin(\frac{\pi}{12}hr)$. The other variables are normalized to the range of [0 1].

TABLE IV:
Input candidates

Input	symbol
Surface insolation	si
Ambient temperature	amb_temp
Sine value of hour	hrsin
Cosine value of hour	hrcos
Humidity	hum
Wind velocity	wv
Wind direction	wd
Enclosure internal temperature	in_temp
Load power	p_load

TABLE V:
Input relevance and mRMR rank

Variable	$d(i,t)$	relevance rank	mRMR rank
amb_temp	0.76	1	1
si	0.62	2	2
hrsin	0.55	3	4
hum	0.46	4	6
wv	0.43	5	5
hrcos	0.38	6	7
in_temp	0.28	7	8
p_load	0.24	8	3
wd	0.15	9	9

Table V summarizes the input importance ranking when only relevance is considered and also when both relevance and redundancy (mRMR) are considered. Several interesting observations can be made regarding the rankings given in Table V.

- Ambient temperature (amb_temp) and surface insolation (si) are the two most important input variables.
- The enclosure inside temperature in_temp is dependent on several factors, therefore its redundancy is high which leads to a relatively low mRMR ranking. It is a good candidate to neglect.
- hrsin ranked higher than hrcos, which indicates that hrsin contains more time information than hrcos. hrcos is a good candidate to neglect.
- The load has low distance correlation to the target, but has a high mRMR rank. This indicates that the load power has low correlation with other input variables, and should not be neglected.

C. ANN structure

A multi-layer perceptron (MLP) type ANN is chosen. The MLP structure is straightforward and uses back propagation as a training method. It has been successfully used to forecast long term and short term energy consumption [24], [25], [26]. The hourly

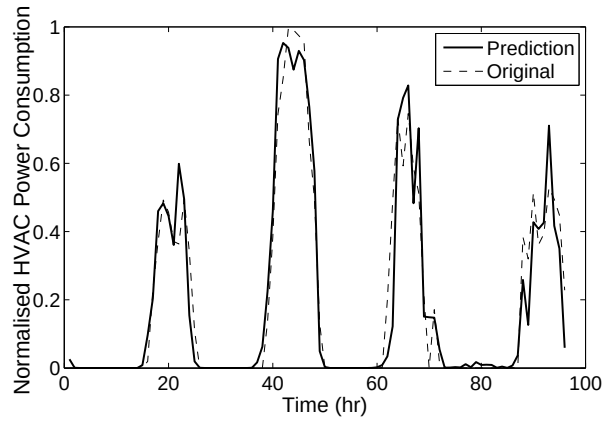

(a) 7 day window

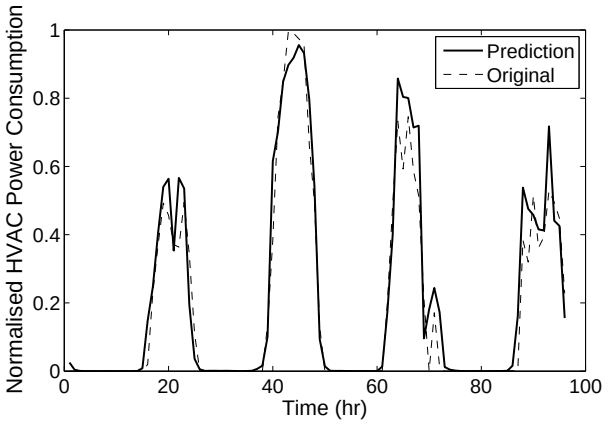

(b) 14 day window

Fig. 7: Simulation result of 7 day and 14 day window

energy consumption of the HVAC is the desired output of the ANN. The ANN has the following structure:

- Network architecture: multilayer perceptron
- Data allocation: sliding window method
- Input variables: hour of the day, solar insolation, humidity, ambient temperature, wind velocity, load power consumption
- Output variable: HVAC hourly energy consumption
- Number of hidden layers: 1
- Number of hidden neurons: 7
- Activation functions: hyperbolic tangent

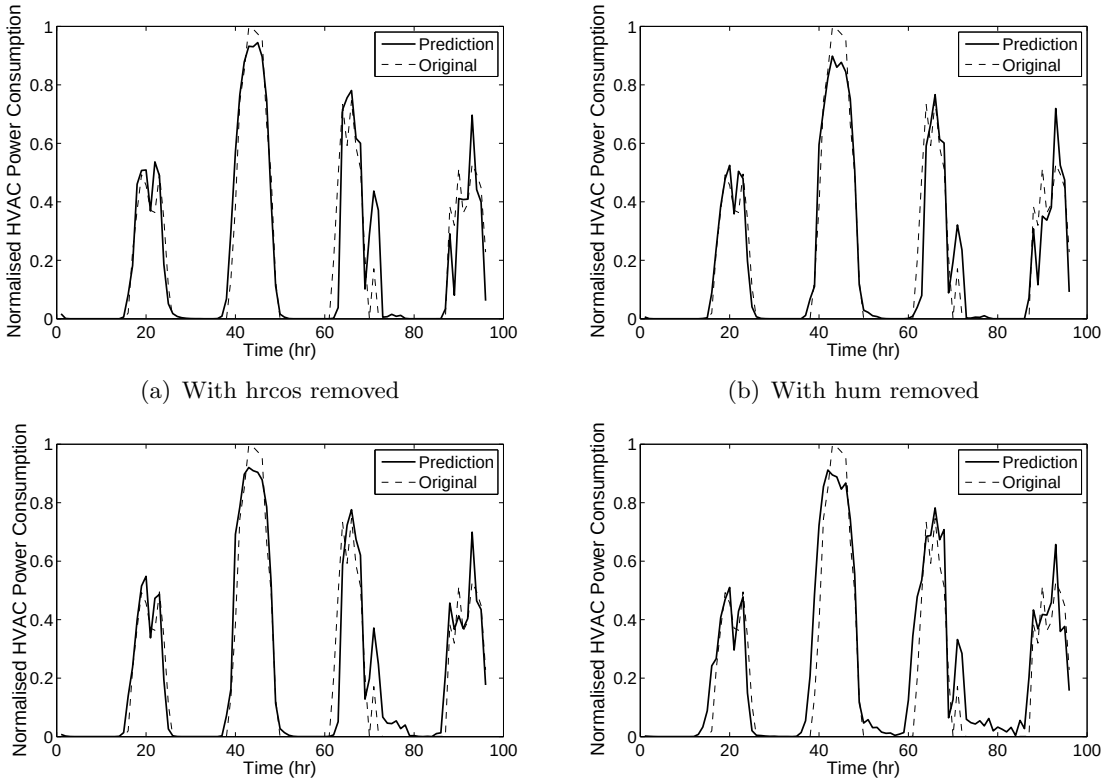

(a) With hrcos removed

(b) With hum removed

(c) With wv removed

(d) With hrsin removed

Fig. 8: Simulation result of 7 day prediction with inputs incrementally removed

V. Model results

Fig. 7 provides a comparison of the predicted HVAC load and the actual HVAC load for a period of 4 days using two different training sets of 7 days (Fig. 7(a)) and 14 days (Fig. 7(b)). For this set of results, all inputs are used. The accuracy of the results is evaluated by the coefficient of variation (CV) and the mean bias error (MBE). For the 7-day window, CV=0.4229 and MBE=0.0006 and for the 14-day window, CV=0.3846 and MBE=0.1072. Distributions with CV < 1 are considered to be low-variance, therefore both training sets are considered to be appropriate. However, since the MBE of the 7-day training set is much smaller than the 14-day training set, a 7-day training set is better suited. This is probably due to greater variations in weather over longer periods of time.

To improve computational efficiency, the number of inputs is reduced. To see the significance of each input, the number of inputs is decremented with the lowest

mRMR removed first. Fig. 8 shows the result and Table VI gives the CV and MBE values. As expected, error increases when effective inputs are ruled out one by one. This effect is shown in Fig. 8. Even with four of the inputs removed, the results are still relatively accurate.

TABLE VI:
CV and MBE values

Input removed	CV	MBE
none	0.4229	0.0006
hum	0.4275	-0.0177
hrcos	0.4928	-0.0218
wv	0.4578	0.0600
hrsin	0.5346	0.1888

VI. Conclusions

To deploy energy storage within a microgrid with confidence, the impact of the balance of plant of the ESS must be considered. It is necessary to be accurately model all parasitic losses in the system. One of the largest components of the parasitic losses are those losses associated with environment controls required to keep the electrochemical reaction within its safe and effective operating region. Due to the difficulty in deriving a mathematical model for the environmental control losses, we have proposed a heuristic ANN-based model. The simulation results indicate that the ANN model can effectively predict the HVAC losses when trained with an appropriate set of representative data. In the future, the model will need to be adaptively updated to incorporate seasonal changes in solar insolation and temperature.

References

[1] "Smart grid: an introduction." [Online].

[2] X. Liu and W. Wang, "VRLA battery system reliability and proactive maintenance," in *Telecommunications Energy Conference (INTEC), 32nd International*, 2010, pp. 1–7.

[3] T. Kaizuka and T. Sasaki, "Evaluation of control maintaining electric power quality by use of rechargeable battery system," in *IEEE Power Engineering Society Winter Meeting, 2001*, vol. 1. IEEE, 2001, pp. 88–93 vol. 1.

[4] T. Shigematsu, T. Kumamoto, H. Deguchi, and T. Hara, "Applications of a vanadium redox-flow battery to maintain power quality," in *Transmission and Distribution Conference and Exhibition 2002: Asia Pacific. IEEE/PES*, vol. 2. IEEE, Oct. 2002, pp. 1065–1070 vol. 2.

[5] C. Blanc and A. Rufer, "Multiphysics and energetic modeling of a vanadium redox flow battery," in *IEEE International Conference on Sustainable Energy Technologies, 2008. ICSET 2008.* IEEE, Nov. 2008, pp. 696–701.

[6] J. Chahwan, C. Abbey, and G. Joos, "VRB modelling for the study of output terminal voltages, internal losses and performance," in *Electrical Power Conference, 2007. EPC 2007. IEEE Canada.* IEEE, Oct. 2007, pp. 387–392.

[7] X. Qiu, T. A. Nguyen, M. L. Crow, J. Guggenburger, and A. C. Elmore, "A field validated model of a vanadium redox flow battery for microgrids," *IEEE Transactions on Smart Grid*, vol. 5, no. 4, July 2014.

[8] H. A. Kiehne, *Batteries Technology Handbook*, 2ed. Expert Verlag, Renningen-Malmsheim, Germany, 2003.

[9] American Society of Heating, Refrigerating, and Air-Conditioning Engineers, *2009 ASHRAE handbook fundamentals.* American Society of Heating, Refrigerating and Air-Conditioning Engineers, 2009.

[10] F. C. McQuiston, J. D. Parker, and J. D. Spitler, *Heating, ventilating, and air conditioning: analysis and design.* Hoboken, N.J.: John Wiley & Sons, 2005.

[11] H. Zhao and F. Magouls, "A review on the prediction of building energy consumption," *Renewable and Sustainable Energy Reviews*, vol. 16, no. 6, pp. 3586–3592, August 2012.

[12] S. A. Kalogirou, C. C. Neocleous, and C. N. Schizas, "Building heating load estimation using artificial neural networks," vol. 8. Citeseer, 1997, p. 14.

[13] B. B. Ekici and U. T. Aksoy, "Prediction of building energy consumption by using artificial neural networks," *Advances in Engineering Software*, vol. 40, no. 5, pp. 356–362, May 2009.

[14] A. Azadeh, S. F. Ghaderi, and S. Sohrabkhani, "Annual electricity consumption forecasting by neural network in high energy consuming industrial sectors," *Energy Conversion and Management*, vol. 49, no. 8, pp. 2272–2278, August 2008.

[15] S. Javeed Nizami and A. Z. Al-Garni, "Forecasting electric energy consumption using neural networks," *Energy Policy*, vol. 23, no. 12, pp. 1097–1104, December 1995.

[16] R.-S. Liu, L. Zhang, X. Sun, H. Liu, and J. Zhang, Eds., *Electrochemical Technologies for Energy Storage and Conversion, Volume 1&2*, January 10, 2012.

[17] T. A. Nguyen, X. Qiu, J. D. Guggenberger II, M. L. Crow, and A. C. Elmore "Performance Characterization for Photovoltaic-Vanadium Redox Battery Microgrid Systems," *IEEE Transactions on Sustainable Energy*, Early Access.

[18] J. Guggenberger, A. Elmore, J. Tichenor, and M. Crow, "Performance prediction of a vanadium redox battery for use in portable, scalable microgrids," *IEEE Transactions on Smart Grid*, vol. 3, no. 4, pp. 2109–2116, 2012.

[19] Y. A. Cengel, *Introduction to thermodynamics and heat transfer.* Dubuque, IA: McGraw-Hill, 2008.

[20] T. Defraeye, B. Blocken, and J. Carmeliet, "Convective heat transfer coefficients for exterior building surfaces: Existing correlations and cfd modelling," *Energy Conversion and Management*, vol. 52, no. 1, p. 512–522, 2011.

[21] R. May, G. Dandy, and H. Maier, "Review of input variable selection methods for artificial neural networks," *Artificial neural networksmethodological advances and biomedical applications. InTech, Croatia. doi*, vol. 10, p. 16004, 2011.

[22] D. W. Scott, *Multivariate density estimation: theory, practice, and visualization.* New York: Wiley, 1992.

[23] C. Ding and H. Peng, "Minimum redundancy feature selection from microarray gene expression data," in *Proceedings of the 2003 IEEE Bioinformatics Conference, 2003. CSB 2003*, August 2003, pp. 523–528.

[24] A. Khotanzad, R.-C. Hwang, A. Abaye, and D. Maratukulam, "An adaptive modular artificial neural network hourly load forecaster and its implementation at electric utilities," *IEEE Transactions on Power Systems*, vol. 10, no. 3, pp. 1716–1722, 1995.

[25] O. Mohammed, D. Park, R. Merchant, T. Dinh, C. Tong, A. Azeem, J. Farah, and C. Drake, "Practical experiences with an adaptive neural network short-term load forecasting system," *IEEE Transactions on Power Systems*, vol. 10, no. 1, pp. 254–265, 1995.

[26] J. Yang, H. Rivard, and R. Zmeureanu, "On-line building energy prediction using adaptive artificial neural networks," *Energy and Buildings*, vol. 37, no. 12, pp. 1250–1259, December 2005.

Xin Qiu received his BS degree of electrical engineering in 2007 from Shanghai Jiaotong University and worked as a design engineer in Cooper Power Systems in Shanghai from 2007 to 2009. He is currently a graduate research assistant at Missouri University of Science and Technology. His research interests are flow battery energy storage systems, renewable energy applications, and microgrid control.

M. L. Crow (S'83–M'90–SM'94–F'10) received the B.S.E. degree from the University of Michigan, Ann Arbor, and the Ph.D. degree from the University of Illinois, Urbana/Champaign. She is the F. Finley Distinguished Professor of Electrical Engineering at the Missouri University of Science & Technology. Her research interests include computational methods for dynamic security assessment and the application of energy storage in bulk power systems.

A. C. Elmore received a B.S. degree in geological engineering from the University of Missouri-Rolla and his M.S. and Ph.D. degrees in civil engineering from the University of Arizona, Tucson. He was employed as a Consulting Engineer with URS Group, Overland Park, KS, where he specialized in green and sustainable environmental remediation. He is currently a Professor of Geological Engineering at the Missouri University of Science & Technology, Rolla.

Paper III

Heterogeneous Energy Storage Optimization for Microgrids

Xin Qiu, Tu A. Nguyen, M. L. Crow, *IEEE Fellow*
Department of Electrical and Computer Engineering
Missouri University of Science and Technology, Rolla, MO 65401

Abstract

In future microgrids, it will be common for different types of energy storage systems to coexist on the grid. Because each storage system has different capabilities and capacities, they will complement each other and be able to achieve more efficient and reliable results than if only a single type of system were used. However, integrating multiple types of storage comes with several implementation challenges. Existing control techniques used to charge and discharge different technologies are not sufficient to accommodate the electrochemical (or mechanical) differences. In this paper, we propose an interconnection topology and a reinforcement learning-based algorithm to optimize the coordination of different ESS in a microgrid.

I. Introduction

The flexible structure and large penetration of distributed energy resources (DER) in microgrids give rise to different operation and control strategies than those of the traditional power systems [1]. Having a diversity of resources in a microgrid is more economic, more secure, and sustainable than relying on a single technology resource; therefore, the future microgrid will most likely rely on a mixture of renewable and nonrenewable types of distributed generation (DG) as well as energy storage. In the future distribution microgrid, multiple types of DG technology and energy storage systems will be connected simultaneously. But coordinating multiple energy storage

types can be challenging due to their differences in response times, control mechanics, and charging/discharging efficiencies. The resource variability from the distributed solar PV and wind turbines makes it even harder to manage energy balance. Most research to date has considered only a single energy storage technology at a time and assumes that they operate similarly. However, different types of energy storage technologies have different capabilities, which can be highly beneficial if they are coordinated properly, so that one type of energy storage characteristics complements the others. Due to the combination of renewable energy variation and the uncertainty of local loads, energy storage becomes attractive for maintaining a high and relatively constant load factor and reliable consumer service.

A variety of battery types can be expected to be deployed in the modern microgrid, each of them having advantages and disadvantages. Traditional lead acid batteries have the advantage of low cost but suffer from a limited useful lifetime when deep-cycled on a daily basis and low energy density at a high mass ratio [2]. Pumped hydro energy storage or compressed air energy storage also provide high power and long duration, but they have the drawback of site-dependence. Li-on batteries are a promising technology due to their high efficiency, energy density, and a low self-discharge rate. However, they are more cost effective for transportation applications and less for grid-scale applications [3, 4]. For these reasons, flow batteries, and specifically Vanadium redox batteries (VRB), are good candidates to fill the void for high power and energy dense applications due to their favorable characteristics such as independent energy capacity and power output, accurate measurement of state of charge and fast response time.

A microgrid with only one energy storage system (ESS) has the advantage of simplicity of control, but may suffer from low efficiency and degradation of lifetime by forcing the ESS to accommodate all power and energy needs. For example, in [5] it was shown that a commercial charge controller designed for lead-acid batteries could not exploit the full potential capability of the deployed VRB, especially at low loads. A microgrid with multiple identical ESS can provide more flexibility, but the

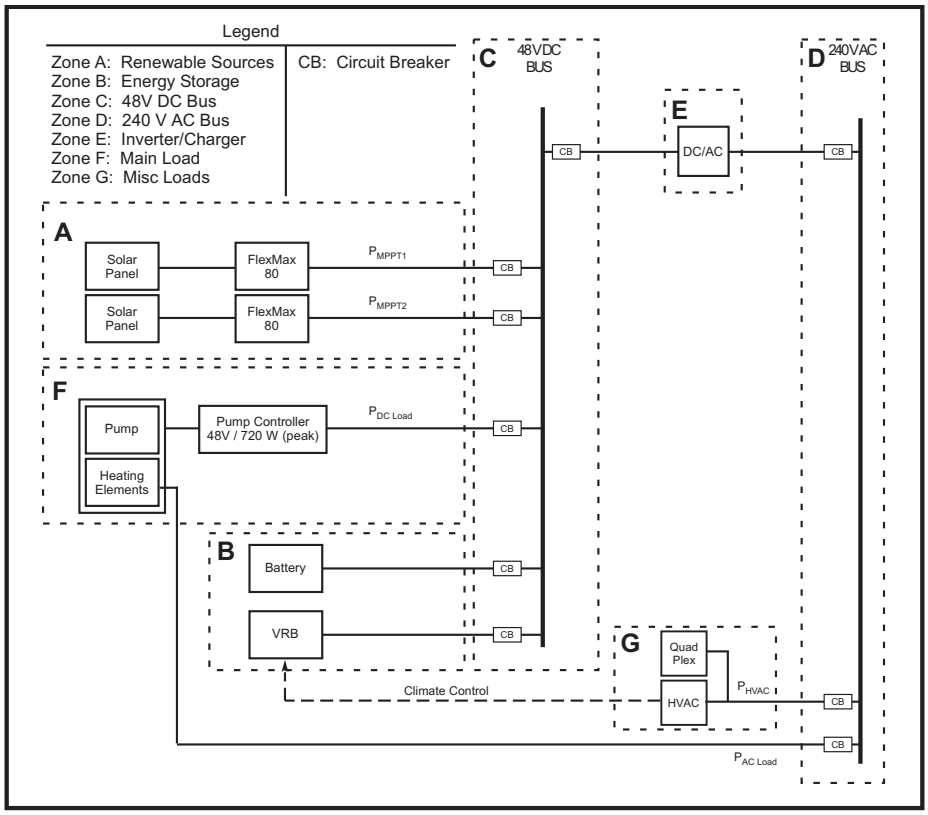

Fig. 1: Field Microgrid System

individual units may still suffer from many of the same constraints. By introducing multiple types of ESS, a wide range of operating conditions can be met at increased efficiencies. However, heterogeneous ESS suffer from the challenges of incompatible charge controllers, different power/energy versus efficiency characteristics, and different response rates. This result leads to the supposition that the deployment of a variety of ESS could potentially provide better efficiency and reliability if properly interleaved and controlled.

Microgrid control can be divided hierarchically into low level and high level controls. Low level control includes regulating the voltage, current and frequency of the power grid and is typically achieved at the power electronics interface. For instance, the maximum power point tracker (MPPT), which is often used to optimize the power output of solar panels or wind turbine generators, controls the current flow. Higher level controls set the control references for the lower level, based on a variety of

considerations such as maintaining an energy reserve, maximizing the overall system efficiency, or optimizing the local power production based on the market price if net metering is presumed.

Most commercially available battery controllers use a form of charge control in which the current input/output of the battery is determined by the bus voltage. In this approach, all batteries connected to the same bus will charge and discharge identically regardless of their individual characteristics. However, to achieve heterogenous control, each ESS must be regulated individually based on a control specific to the capacity, SOC, and type of storage system in use. Two types of converter topologies have been proposed to accomplish this specialized controls: multi-input converters and parallel converters [6–9]. The problematic issue with multi-input converters is that the centralized input limit the geographic freedom in which to locate the batteries. Moreover, once the converter is deployed, it is hard for it to accept new batteries or to exchange one battery type with another. The multi-module parallel converter system is a more flexible and expandable choice, but these converters potentially suffer from stability concerns [10].

Higher level control governs the microgrid power and energy management (PEM). In addition to delivering operational orders to the components, such as synchronization in the grid-tied mode or frequency regulation in the stand-alone mode, load-source matching, voltage and frequency regulation, and fault management, the high level control also sets the long term goals and determines the proper operational strategy. The strategies may include minimization of the overall power losses, fuel costs, or power import from the main grid, among others. Due to the different structure and composition from the traditional power grid, microgrid PEM faces other challenges and difficulties [1]. One of the major challenges is the small scale and volatility of the energy resources, which often requires a considerable level of prediction in the optimization process. Off-line optimization such as dynamic programming (DP) can be algorithmically complex and thorough, but suffers from the inaccuracies inherent in predicting behavior. An online optimization can react to new information, but must

be computationally efficient to run in real-time. Reinforcement learning (RL) in its simplest form can solve the Markov Decision Process (MDP) problem by DP but has a "learning" part of which DP is incapable. There are several RL applications that have been proposed for power system optimization. For example, [11] implemented a multiple object reinforcement learning method to minimize the fuel cost and enhance the voltage stability at the same time. In [12], a multi agent system was proposed to decrease the power losses of a microgrid, but the battery constraints were not very rigid and allowed uncontrolled charging between the batteries. In this paper, **we propose an interconnection topology and an RL-based algorithm to optimize the coordination of different ESS in a microgrid.**

II. Microgrid System Description

The microgrid system used to obtain the field data was the standalone system shown in Fig. 1 deployed at Fort Leonard Wood, Missouri (latitude 37.71°, longitude -92.15°). The system, shown in Fig. 1, included a 6 kW photovoltaic (PV) array consisting of 30 × 200 W solar panels (Brightwatts - BI-156-200W-G27V) connected to two Outback FlexMax 80 charge controllers which charged a 5 kW/20 kWhr VRB (Prudent Energy). The system was loaded with two pumps, several resistive heating elements, and an HVAC system. A 38-cell Prudent Energy VRB rated 5 kW/20 kWh is used for energy storage.

The system is instrumented to measure environmental data including solar insolation and temperature as well as the voltage and current parameters necessary for monitoring, controlling its operation and characterizing its performance. Operational data was are recorded using Campbell Scientific Model CR3000 and CR1000 dataloggers which sample every 5 seconds and average the values over a 1 minute window.

The system was designed to be part of a modular military forward operating base (FOB) system that could operate independently, or as part of an integrated system of microgrids. Although the field validation used data obtained from military base operation, it can be generalized to civilian operation since the loads (pumps, compressors, heating elements, and HVAC) are applicable in multiple situations.

III. Battery Characteristics

A. The vanadium-redox battery

From the VRB circuit shown in Fig. 2 (derived in [5, 13]), the operational power loss of the VRB can be calculated

$$P_{loss} = I_s^2 R_{th} + |V_t I_p| \tag{1}$$

where I_s is the stack current, R_{th} is the equivalent resistance, V_t is the terminal voltage, and I_p is the parasitic current.

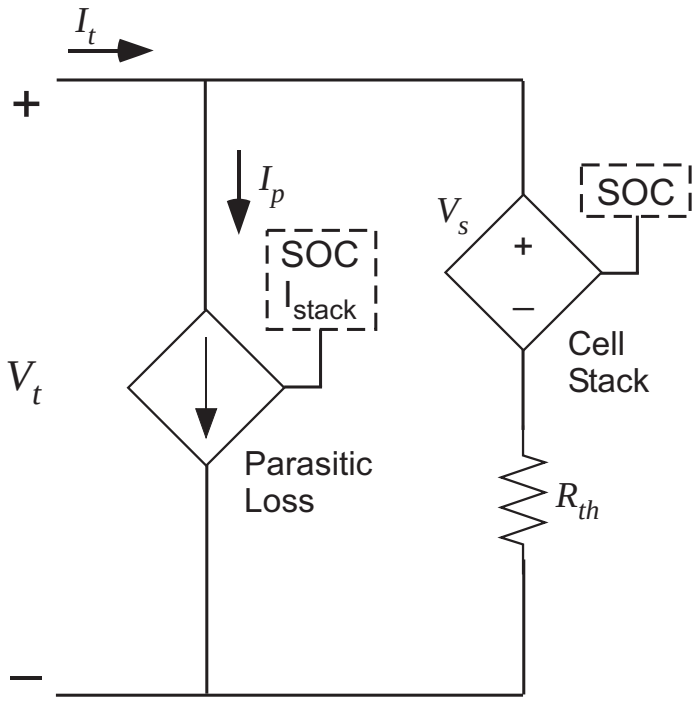

Fig. 2: VRB electrical circuit

The discharge efficiency of the VRB at 50% SOC is shown in Fig. 3 [14]. The slight dip in the curve is due to the point at which the pump moving the electrolyte through the stack changes speed due to the increase in output power requirement.

B. The lead acid battery

The charging and discharging efficiencies can be estimated from Perkert's law [15]:

$$\eta = I^{1-pc} \frac{C_p}{C_{rated}} \tag{2}$$

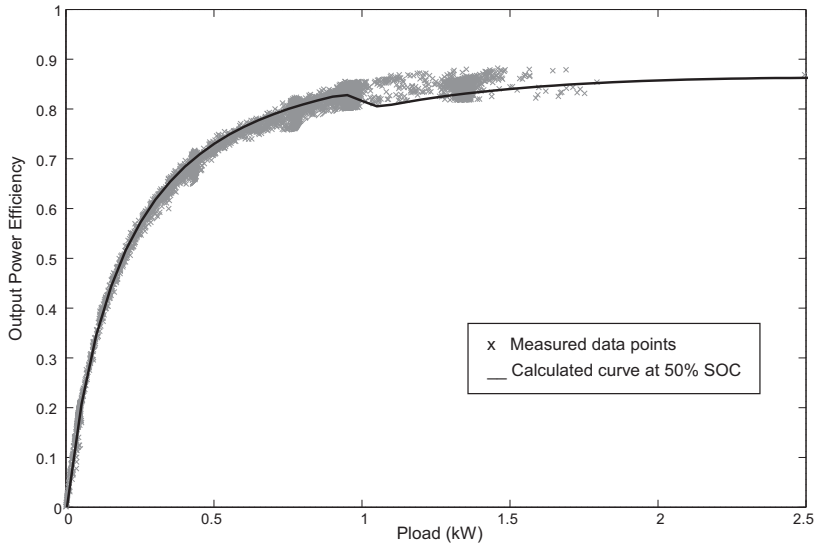

Fig. 3: VRB efficiency (field data versus fitted) at 50% SOC and 25° C

where I (A) is the discharge current, C_{rated} (AHr) is the rated capacity at a certain discharge time T_{rated} (hr), pc is Peukert's coefficient and C_p is Peukert's capacity. For a leadacid battery, the value of pc is typically between 1.1 and 1.3.

By definition Peukert's capacity is calculated by:

$$C_p = I^{pc}T = \left(\frac{C_{rated}}{T_{rated}}\right)^{pc} T_{rated} \tag{3}$$

Since the Peukert's capacity is a constant, the Peukert's coefficient can be derived from:

$$pc = \frac{ln(T_2) - ln(T_1)}{ln(I_1) - ln(I_2)} \tag{4}$$

where I_1 and I_2 are discharge currents at discharge times of T_1 and T_2, which are normally provided by the battery specification.

The ampere-hour counting method is used to estimate the state of charge of the battery [16]. The SOC is then approximated by:

$$SOC = SOC_{t_0} + \frac{1}{C_{rated}} \int_{t_0}^{t} (I - I_{loss}) d\tau \tag{5}$$

where SOC_{t_0} is the initial state of charge and I_{loss} is the current of loss.

The power loss is calculated by the efficiency and terminal power into the battery

$$P_{loss} = P_{term}(1 - \eta) \tag{6}$$

Based on the previous discussion of the battery models, their efficiencies at 50% state of charge are calculated and shown in Fig. 4. Note that lead acid batteries are

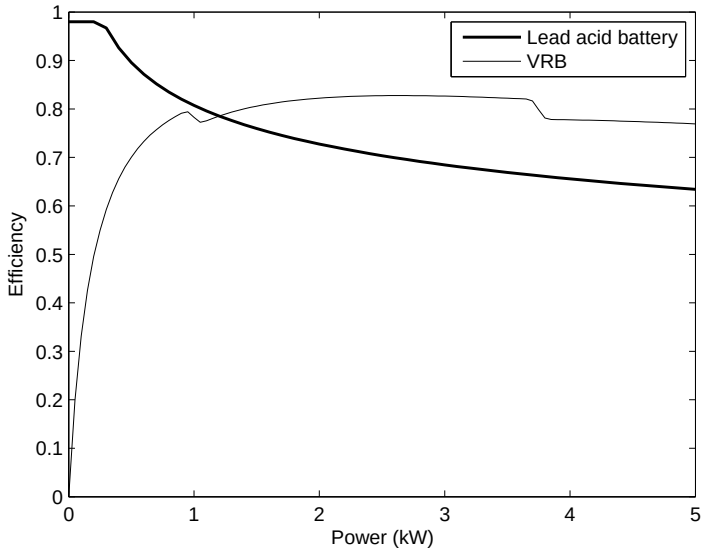

Fig. 4: Battery efficiencies at 50% SOC

most efficient at low powers [17], whereas VRBs are most efficient at high powers. A similar comparison exists for charging as well. By coordinating the charge and discharge between batteries, the optimal system efficiency can be achieved, whereas relying on one type of battery only is less efficient.

C. Battery-Photovoltaics Charging and Discharging Algorithms

Most charge controllers regulate charging current according to a three-stage regime to prevent damage to the battery from over-charging. A typical three-stage charging profile is shown in Fig. 5. These stages are:

- Bulk: when the battery voltage is lower than the *absorb* voltage, the MPPT/charge controller tracks the maximum PV power and charges the battery with the maximum current. The *absorb* voltage level can be set by the user within a pre-defined range.

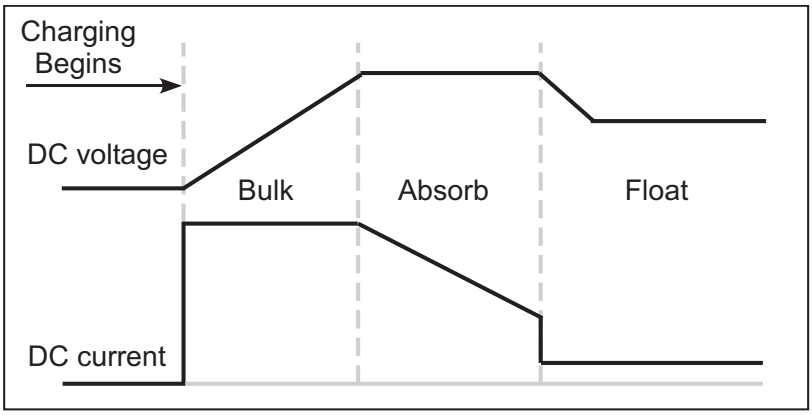

Fig. 5: Typical battery charge regions

- Absorb: when the battery voltage reaches the *absorb* voltage set point, the MPPT/charge controller regulates the battery voltage and charges the battery at a constant voltage.
- Float: when the battery is fully charged, the voltage is decreased and the current is maintained at a small value to account for leakage. This is often known as "trickle charge." A quiescent battery will typically remain in float as long as power is applied to the charger.

This charging scheme is used in the vast majority of commercially available charge controllers.

The drawback to using this particular charging algorithm with a non-lead acid battery, such as a VRB, is that the lead acid battery voltage set points do not map well to the chemistry of other ESS. For example, the charging current is reduced going from *bulk* to *absorb* to protect the lead-acid batteries; however, this is unnecessary with a VRB, which is designed to handle a much higher charging current. The charge controller will prematurely limit the charging current on the VRB. Furthermore, if the VRB is set on float (very low current charge) then it will be very inefficient since this is the poorest operating mode of the VRB due to the ESS parasitics [14].

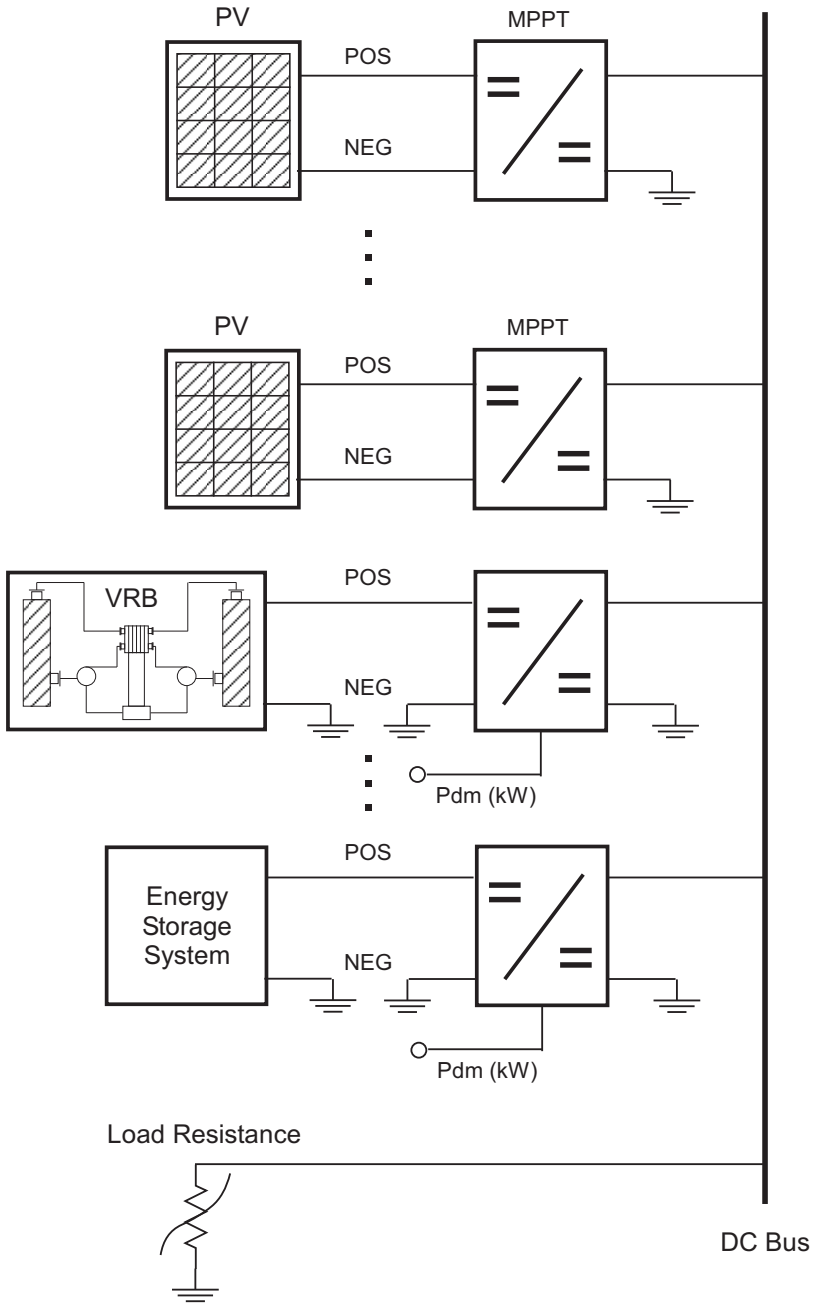

Fig. 6: Microgrid with multiple converter modules

D. Charge Controller Topology

We will use lead acid batteries and VRB systems in this paper because they have dissimilar characteristics and can only be used together effectively if controlled independently. As noted earlier, a coordinated charge control strategy could maximize the operational efficiency of the combined ESS. One interconnection topology for

the microgrid is shown in Fig. 6 in which each ESS is connected through its own inverter to the system. This is the most flexible topology since it allows for each ESS to operate at optimum voltage as well. Power sharing on a DC bus requires a multi-module parallel converter system. Various converter topologies and their control techniques have been developed for several applications [18]-[22]. However, none of these works specifically implemented organized current sharing to maximize the overall system efficiency. We expand on these earlier works to propose both a design and control to maximize the system efficiency. In the parallel converter system, one of the converters is designated as the master while the others are the slave units. The master unit regulates the bus voltage and the slave units regulate the current output of their attached storage device. If the master device goes offline (intentionally or unintentionally disconnected), then a new master is elected from among the slave units. An external high level controller collects information from the solar panels, the load, optimizes the current distribution among the converters, and issues the control settings. A high level control strategy is required to coordinate and optimize the multiple ESS by continuously choosing the most appropriate battery to charge or discharge at any given time based on its own performance characteristics.

IV. Problem Formulation with Reinforcement Learning

Reinforcement learning consists of artificial intelligent techniques that enable an agent to perceive the environment and act optimally. The agent will make the best decisions in a time series from a long term perspective rather than from limited information at specific moments. The learning process involves the agent, the environment, and the interaction between them. The agent takes an action based on the current states and its prior experience with the environment. The action then receives feedback signal, or reward, that indicates the goodness of the action and is added to the cumulative record.

The state, action, transition probability, and reward make the essential elements of a finite Markov Decision Process (MDP)-tuple $\left(S, A, P^a_{s,s'}, R^a_{s,s'}\right)$, where S and A are the finite sets of state and action and $P^a_{s,s'}$ is the probability of the next state s'

in which the current state s and action a are provided [23]:

$$P^a_{s,s'} = Pr(s_{t+1} = s' | s_t = s, a_t = a) \tag{7}$$

$R^a_{s,s'}$ is the expected reward given the next state s' with current state s and action a

$$R^a_{s,s'} = E(r_{t+1} = s' | s_t = s, a_t = a, s_{t+1} = s') \tag{8}$$

The value function and action-value (Q value) function are used to evaluate the goodness of a state. The value function is:

$$U^\pi(s) = E_\pi(R_t | s_t = s) = E\left(\sum_{k=0}^{\infty} \gamma^k r_{t+k+1} | s_t = s\right) \tag{9}$$

where π is the policy, which directs the agent at each state and γ is the discount factor within the range of [0 1]. The discount factor determines whether or not the method favors immediate or delayed rewards. The value function is the expected total reward if the agent starts from s following the policy of π. Derived from its definition, the value function can also be calculated in a more straightforward way as:

$$U^\pi(s) = \sum_a \pi(s,a) \sum_{s'} P^a_{s,s'} \left[R^a_{s,s'} + \gamma U^\pi(s')\right] \tag{10}$$

The action-value function is given by

$$\begin{aligned} Q^\pi(s,a) &= E_\pi(R_t | s_t = s, a_t = a) \\ &= E_\pi\left(\sum_{k=0}^{\infty} \gamma^k r_{t+k+1} || s_t = s, a_t = a\right) \end{aligned} \tag{11}$$

which can also be rewritten as

$$Q^\pi(s,a) = \sum_{s'} P^a_{s,s'} \left[R^a_{s,s'} + \gamma U^\pi(s')\right] \tag{12}$$

Linear programming or dynamic programming can solve the MDP problem, but these solution methods require knowledge of the transition probabilities and value functions [24]. When these are unknown, reinforcement learning can provide a solution approach. The agent will learn these values by simulation and stochastic

approximation, so that the policy mapping can still be accomplished. Of all of the learning methods, the Q-learning method is the most widely used due to its simpler implementation and model free characteristics [23]. The action value function is renewed each time the agent interacts with the environment, such that

$$Q(s,a) \leftarrow (1-\alpha)Q(s,a) + \alpha\Big[r + \gamma \max_{\alpha'} Q(s',a')\Big] \tag{13}$$

It has been proven that for any finite MDP, the Q-learning approach will converge to the optimal policy [25]:

$$\pi(s) = arg\max_{a} Q(s,a) \tag{14}$$

The target of the optimization is to decreases the power losses on energy storage system in the long term. In order to achieve this goal, the agent will try to learn the rational sequence to apply the batteries at a overall higher efficiency. The VRB and lead acid battery modules will be components that the agent controls. The power flow through the batteries will be the difference between the MPPT-based solar power and the load power. As a by-product of the Q-learning method, the load and solar powers do not have to be modeled and therefore actual sampled field data will be used in this development.

- *State space* – The first two components of the state vector are the SOC of the VRB and the lead acid battery. For simplicity and lower dimensionality, the SOC is discretized into three ranges: [0 0.33), [0.33 0.67) and [0.67 1]. The third component is the terminal power of battery group, divided into two ranges. The range division point is where the two battery efficiency curves intersect each other, which is set to 1.2 kW in this study.

$$\mathcal{S} : \{SOC_{vrb}, SOC_{la}, P_d\}$$

- *Action space* – The action space consists of the instructions to turn on or off the batteries.

$$\mathcal{A} : \{A_{vrb}, A_{la}\}$$

- *Instant reward* – Generally, the combined battery system power losses would be used to calculate the instant reward. If the battery is available (within SOC and power rating ranges), the reward is defined as the losses on that battery given the terminal power. Otherwise, the reward is defined as the terminal power. Thus the agent is punished to a greater extent if a particular battery is needed but not available.

$$\mathcal{R}: \begin{cases} -|P_{loss}| \text{ if the battery is available} \\ -|P_d| \text{ otherwise} \end{cases}$$

There are several constraints the system must comply with:

- The battery module assumes the power difference between the power source and the load

$$P_{batt} = P_s - P_{load}$$

- The batteries must remain within the allowable state of charge

$$SOC_{min} < SOC_{batt} < SOC_{max}$$

- The battery must be charged or discharged within its power rating

$$\begin{cases} P_{d,min} < P_{batt} < P_{d,max} \\ P_{c,min} < P_{batt} < P_{c,max} \end{cases}$$

The step by step algorithm is given in Algorithm 1.

V. Results and Discussion

Table I provides the basic VRB rated operating data. The capacity range of the Prudent Energy VRB is specified as 20kWh at a SOC of 73% and 0kWh at a SOC of 20%. It can be charged to a maximum voltage of 56.5 V and discharged to a minimum voltage of 42 V. The lead acid battery module is composed of the 4 PVX-1080T in series. PVX-1080T is from SunXtender and its parameters can be found in Table II.

Algorithm 1 Q-learning for batteries

procedure
Initialize the model of VRB and lead acid battery;
Import the data of the source and the load power;
Parameterize the agent;
Initialize the $Q(s, a)$ table;

Observe s
repeat
Pick the battery to allocate based on s and Q table,
using ϵ-greedy selection method;
Observe the power loss, calculate the reward r;
Update $Q(s, a)$;
$s \leftarrow s'$;
until end of operation

TABLE I:
VRB operating data

Rated power	5 kW
Rated energy	20 kWh
Maximum voltage	59 V
Minimum voltage	42 V
Maximum current	140 A
Minimum current	125 A

The solar power data were sampled at the point after the MPPT. The solar power was sampled every 5 seconds and averaged over a 1 minute time window. The load data is collected in a similar way. The difference between the PV power and load (P_{diff}) is shown in Fig. 7. When the power is positive, the PV panels are producing more than the load requires and the batteries can charge. When the power is negative,

TABLE II:
Lead-Acid PVX-1080T operating data

Voltage	12V
Nominal capacity, 24 hour rate	108Ahr
Maximum current	540A
Perkeut's coefficient	1.15

TABLE III:
Learning parameters

Learning rate (α)	0.01
Discount rate (γ)	0.98
ϵ (ϵ-greedy)	0.9
Q table dimension	$3 \times 3 \times 2$

the batteries must discharge to satisfy the load. In this example, the average of $P_{diff} > 0$ which indicates that the PV panels are sized sufficiently large to fully charge the batteries most days. With the battery characteristics and sampling rate considered, the time horizon of the reinforcement learning is also discretized by minutes. The other learning parameters are shown in Table III. The first approach to scheduling

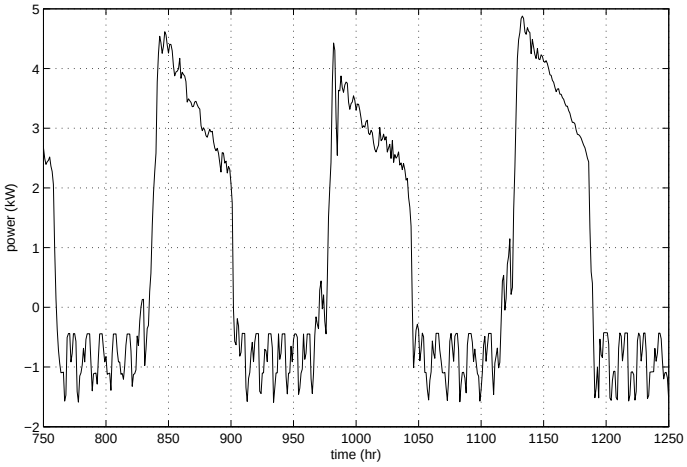

Fig. 7: The power demand of the battery module over 3 typical days

the batteries' charge and discharge periods is a "greedy" method, in which the battery with the highest efficiency (based on SOC) at any decision point (every ten minutes) is selected to be charged or discharged (depending on whether P_{diff} is positive or negative). The scheduling of the lead-acid and VRB are shown in Fig. 8. Note that the lead-acid battery (light gray) is the first to discharge, because at low powers it is more efficient than the VRB. During the morning, when the PV power becomes available, the VRB is the first to charge because it is more efficient at high charge rates. Fig.

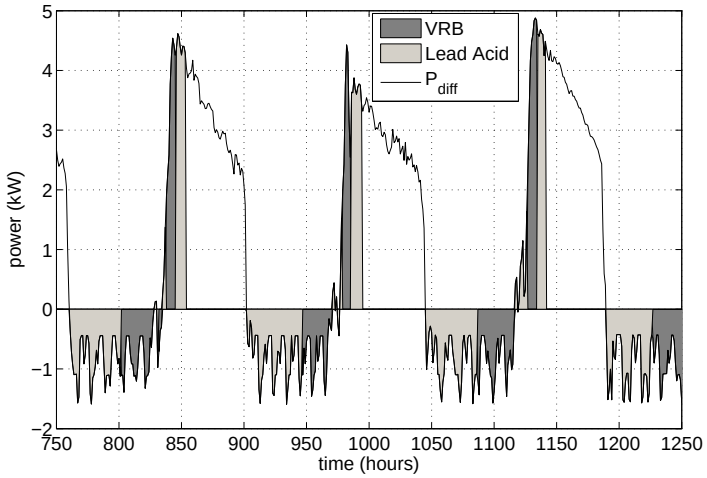

Fig. 8: Charge and Discharge of the Greedy Method

9 shows the results of the proposed Q-learning method. In this case, the VRB and the lead-acid (LA) battery charge and discharge in a non-discernible pattern that is governed by the Q-learning method. At first consideration, this may not appear to provide superior performance, but it does indeed lead to lower system losses by increasing the overall efficiency of the combined VRB-LA system. The power losses

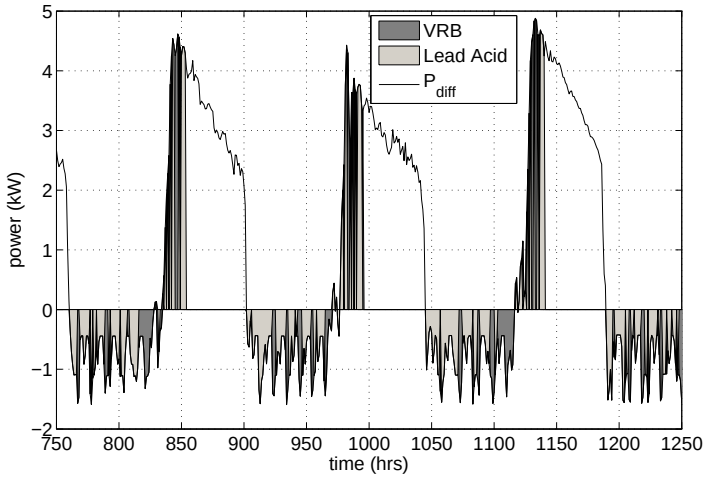

Fig. 9: Charge and Discharge of the Q-Learning Method

of the battery configurations are shown in Fig. 10. Note that as a standalone system, the LA battery is more efficient in this application than the VRB. However, by

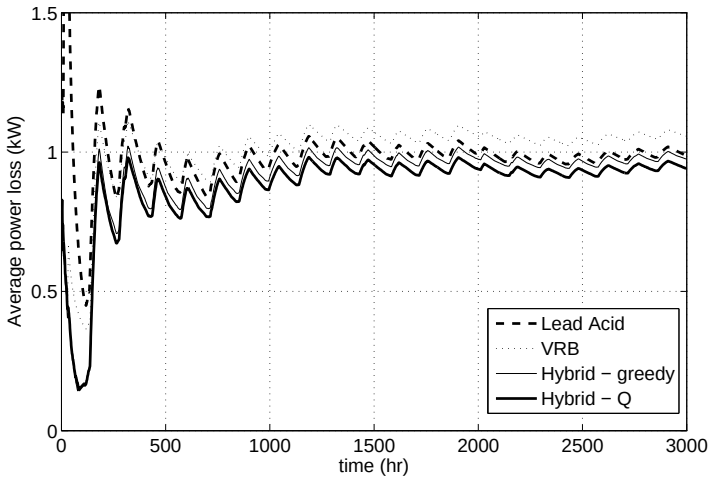

Fig. 10: Losses of different energy storage operating scenarios

combining the lead-acid batteries with the VRB, the efficiency of the hybrid system is improved and the power losses are lowered. Furthermore, by implementing the Q-learning method, the losses are the lowest (designated as Q-Hybrid in Fig. 10). Note that as time increases, the losses also decrease because the system "learns" and gradually adjusts the scheduling algorithm to maximize the reward function.

The superiority of the Q-learning algorithm can be seen most effectively when considering days in which the PV power is variable. Consider the greedy scheduling of the day shown in Fig. 11. The greedy method chooses the LA battery first, then switches to the VRB when the power increases. When the PV power drops it switches back to the LA, then back to the VRB when the PV increases. The unfortunate part of this approach is that the VRB is already fully charged when the PV power peaks and the LA battery must be charged. Thus the LA is charged at high power and low efficiency, whereas it would have been better to charge the VRB at high power when it is most efficient.

Contrast the greedy method with the Q-learning method scheduling shown in Fig. 12. In this figure, it can be observed that the Q-learning method effectively delays much of the VRB charging until later in the day, thus charging it at higher power when it is more efficient and front loads the lead-acid during lower power charging.

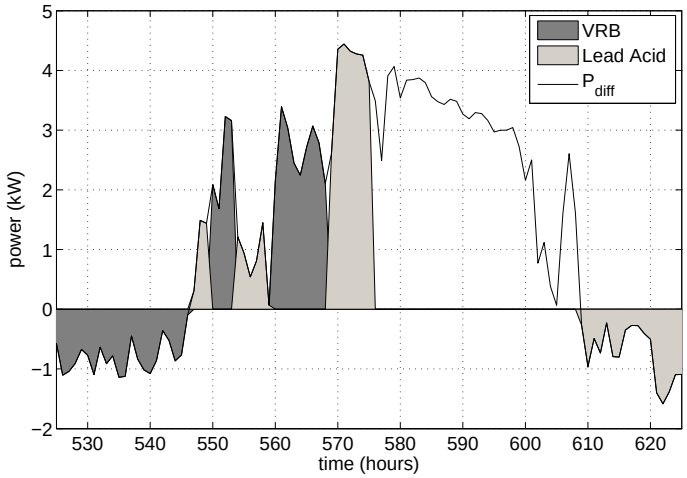

Fig. 11: Charge and Discharge of the Greedy Method - variable PV

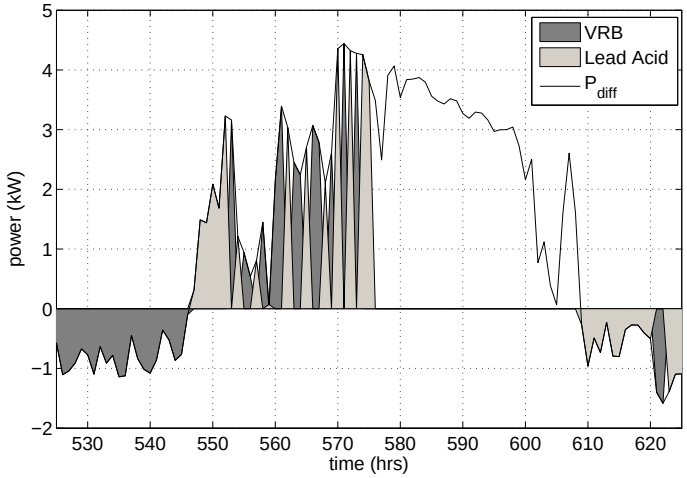

Fig. 12: Charge and Discharge of the Q-learning Method - variable PV

VI. Conclusion

It was shown that commercially available charge controllers typically sold with PV systems are not well-suited for use with energy storage systems other than lead-acid batteries. To counter this effect, a new master-slave control was proposed such that two or more heterogeneous energy storage systems can be used and controlled. A reinforcement learning strategy is proposed to coordinate different batteries in a microgrid. By controlling the charge and discharge periods of the different battery

systems, better system efficiency can be achieved. It was shown that a hybrid system can exploit the differences in operation between the two storage types to achieve better efficiency than either of the battery systems alone. Although the reinforcement learning strategy approach was applied to a hybrid system of two batteries, the methodology can be generalized to handle multiple types of batteries as long as their efficiency profiles are known.

Acknowledgements

The authors gratefully acknowledge the financial support of the US National Science Foundation under ERC award EEC-08212121 and the US Department of Energy under SunShot award DE-0006341.

References

[1] F. Katiraei, R. Iravani, N. Hatziargyriou, and A. Dimeas, "Microgrids management," *IEEE Power and Energy Magazine*, vol. 6, no. 3, pp. 54–65, May 2008.

[2] X. Liu and W. Wang, "VRLA battery system reliability and proactive maintenance," in *Telecommunications Energy Conference (INTEC), 32nd International*, 2010, pp. 1–7.

[3] K. Divya and J. Ostergaard, "Battery energy storage technology for power systemsn overview," *Electric Power Systems Research*, vol. 79, no. 4, pp. 511–520, April 2009.

[4] H. L. Ferreira, R. Garde, G. Fulli, W. Kling, and J. P. Lopes, "Characterisation of electrical energy storage technologies," *Energy*, vol. 53, pp. 288–298, May 1, 2013.

[5] X. Qiu, T. A. Nguyen, M. L. Crow, J. Gugenburger, and A. C. Elmore, "A field validated model of a vanadium redox flow battery for microgrids," *IEEE Transactions on Smart Grid*, 2014.

[6] L. Dixon, "Average current mode control of switching power supplies," in *Unitrode Power Supply Design Seminar Manual SEM700*, 1990.

[7] B. G. Dobbs and P. L. Chapman, "A multiple-input dc-dc converter topology," *IEEE Power Electronics Letters*, vol. 1, no. 1, pp. 6–9, 2003.

[8] J. Abu-Qahouq, M. Batarseh, L. Huang, and I. Batarseh, "Analysis and small signal modeling of a non-uniform multiphase buck converter," in *IEEE Power Electronics Specialists Conference, 2007. PESC 2007.* IEEE, 17-21 June 2007, pp. 961–967.

[9] M. Gavris, O. Cornea, and N. Muntean, "Multiple input dc-dc topologies in renewable energy systems - a general review," in *2011 IEEE 3rd International Symposium on Exploitation of Renewable Energy Sources (EXPRES).* IEEE, 3-11-2011, pp. 123–128.

[10] S. Sudhoff, S. Glover, P. Lamm, D. Schmucker, and D. Delisle, "Admittance space stability analysis of power electronic systems," *Aerospace and Electronic Systems, IEEE Transactions on*, vol. 36, no. 3, pp. 965–973, 2000.

[11] H. Liao, Q. Wu, and L. Jiang, "Multi-objective optimization by reinforcement learning for power system dispatch and voltage stability," in *Innovative Smart Grid Technologies Conference Europe (ISGT Europe), 2010 IEEE PES*, October 2010, pp. 1–8.

[12] F. Lauri, G. Basso, J. Zhu, R. Roche, V. Hilaire, and A. Koukam, "Managing power flows in microgrids using multi-agent reinforcement learning," *Agent Technologies in Energy Systems (ATES)*, 2013.

[13] J. Chahwan, C. Abbey, and G. Joos, "VRB modelling for the study of output terminal voltages, internal losses and performance," in *Electrical Power Conference, 2007. EPC 2007. IEEE Canada.* IEEE, Oct. 2007, pp. 387–392.

[14] T. Nguyen, X. Qiu, J. D. Guggenberger, M. L. Crow, and A. C. Elmore, "Performance characterization for photovoltaic-vanadium redox battery microgrid systems," *IEEE Transactions on Sustainable Energy*, 2013, vol. 5, no. 4, October 2014.

[15] T. A. Nguyen and M. Crow, "Optimization in energy and power management for renewable-diesel microgrids using dynamic programming algorithm," in *2012*

IEEE International Conference on Cyber Technology in Automation, Control, and Intelligent Systems (CYBER), May 2012, pp. 11–16.

[16] S. Piller, M. Perrin, and A. Jossen, "Methods for state-of-charge determination and their applications," *Journal of Power Sources*, vol. 96, no. 1, pp. 113–120, June 1, 2001.

[17] J. W. Stevens and G. P. Corey, "A Study of Lead-Acid Battery Efficiency Near Top-of-Charge and the Impact on PV System Design," 1996 Photovoltaics Specialists Conference, Washington DC, May 1996.

[18] J. A. A. Qahouq and L. Huang, "Power converter with gradient power architecture and non-uniform current sharing," in *Telecommunications Energy Conference, 2006. INTELEC '06. 28th Annual International.* IEEE, Sep. 2006, pp. 1–8.

[19] P. T. Krein, J. W. Kimball, and B. T. Kuhn, "Non-droop methods for context-sensitive sharing in multi-module switching converters," in *Control and Modeling for Power Electronics, 2008. COMPEL 2008. 11th Workshop on*, 2008.

[20] I. Kondratiev, E. Santi, R. Dougal, and G. Veselov, "Synergetic control for m-parallel connected dc-dc buck converters," in *Power Electronics Specialists Conference, 2004. PESC 04. 2004 IEEE 35th Annual*, vol. 1, 2004, p. 182–88.

[21] V. Thottuvelil and G. Verghese, "Analysis and control design of paralleled dc/dc converters with current sharing," *IEEE Transactions on Power Electronics*, vol. 13, no. 4, pp. 635–644, July 1998.

[22] P. S. Shenoy and P. T. Krein, "Local control of an isop push-pull converter with uneven load sharing," in *Power and Energy Conference at Illinois (PECI), 2010.* IEEE, 12-13 Feb. 2010, pp. 70–76.

[23] R. S. Sutton and A. G. Barto, *Reinforcement Learning: An Introduction.* A Bradford Book, 1998-03-01.

[24] P. Norvig, *Artificial Intelligence: A Modern Approach*, 3rd ed. Upper Saddle River: Prentice Hall, December 11, 2009.

[25] C. Watkins and P. Dayan, "Q-Learning," *Machine Learning*, vol. 8, pp. 279–292, 1992.

Xin Qiu received his BS degree of electrical engineering in 2007 from Shanghai Jiaotong University and worked as a design engineer in Cooper Power Systems in Shanghai from 2007 to 2009. He is currently a graduate research assistant at Missouri University of Science and Technology. His research interests are flow battery energy storage systems, renewable energy applications, and microgrid control.

Tu A. Nguyen received his B.S degree from Hanoi University of Science and Technology, Hanoi, Vietnam in 2007. He worked as a Power Transformer Test Engineer in ABBs High Voltage Test Department in Vietnam from 2008 to 2009. He is currently a PhD. candidate at Missouri University of Science and Technology. His research interests include microgrid system modeling/analysis and power electronics applications in microgrid systems.

M. L. Crow (S'83–M'90–SM'94–F'10) received the B.S.E. degree from the University of Michigan, Ann Arbor, and the Ph.D. degree from the University of Illinois, Urbana/Champaign. She is the F. Finley Distinguished Professor of Electrical Engineering at the Missouri University of Science & Technology. Her research interests include computational methods for dynamic security assessment and the application of energy storage in bulk power systems.

SECTION
2. CONCLUSIONS

To deploy energy storage within a microgrid with confidence, it is necessary to accurately model all parasitic losses in the system, including the impact of the balance of plant of the ESS. One of the parasitic loss is the circulation pump of VRB. It was characterized as a function of the VRB state of charge and the stack current. The modeled current was experimentally validated against the measured current. The VRB equivalent resistance was also experimentally obtained. Another major parasitic loss is associated with environment controls required to keep the electrochemical reaction within its safe and effective operating region. Due to the difficulty in deriving a mathematical model for the environmental control losses, we have proposed a heuristic ANN-based model. The simulation results indicate that the ANN model can effectively predict the HVAC losses when trained with an appropriate set of representative data. In the future, the model will need to be adaptively updated to incorporate seasonal changes in solar insolation and temperature.

It was also shown that commercially available charge controllers typically sold with PV systems are not well-suited for use with energy storage systems other than lead-acid batteries. To counter this effect, a new master-slave control was proposed such that two or more heterogeneous energy storage systems can be used and controlled. A reinforcement learning strategy is proposed to coordinate different batteries in a microgrid. By controlling the charge and discharge periods of the different battery systems, better system efficiency can be achieved. It was shown that a hybrid system can exploit the differences in operation between the two storage types to achieve better efficiency than either of the battery systems alone. Although the reinforcement learning strategy approach was applied to a hybrid system of two batteries, the

methodology can be generalized to handle multiple types of batteries as long as their efficiency profiles are known.

REFERENCES

[1] Department of Energy, "Smart grid: an introduction." [Online]. Available: `http://energy.gov/oe/downloads/smart-grid-introduction`

[2] J.D. Guggenberger, A.C. Elmore, J.L. Tichenor, and M.L. Crow. Performance prediction of a vanadium redox battery for use in portable, scalable microgrids. *IEEE Transactions on Smart Grid*, 3(4):2109–2116, 2012.

[3] Xiyu Liu and Wei Wang, "VRLA Battery System Reliability and Proactive Maintenance," *32nd Int'l Telecommunications Energy Conference*, Orlando, FL, June 2010.

[4] H. L. Ferreira, R. Garde, G. Fulli, W. Kling, and J. P. Lopes, "Characterisation of electrical energy storage technologies," *Energy*, vol. 53, pp. 288–298, May 1, 2013.

[5] K. Divya and J. stergaard, "Battery energy storage technology for power systems overview," *Electric Power Systems Research*, vol. 79, no. 4, pp. 511–520, April 2009.

[6] Thomas Reddy, *Linden's Handbook of Batteries, 4th Edition.* McGraw-Hill Professional, 4 edition, 2010-10-27.

[7] Ru-Shi Liu, Lei Zhang, Xueliang Sun, Hansan Liu, and Jiujun Zhang, editors. *Electrochemical Technologies for Energy Storage and Conversion, Volume 1&2.* January 10, 2012.

[8] C. Blanc and A. Rufer. Multiphysics and energetic modeling of a vanadium redox flow battery. In *IEEE International Conference on Sustainable Energy Technologies, 2008. ICSET 2008*, pages 696–701. IEEE, November 2008.

[9] J. Chahwan, C. Abbey, and G. Joos. VRB modeling for the study of output terminal voltages, internal losses and performance. In *Electrical Power Conference, 2007. EPC 2007. IEEE Canada*, pages 387–392. IEEE, October 2007.

[10] K. W. Knehr and E. C. Kumbur. Open circuit voltage of vanadium redox flow batteries: Discrepancy between models and experiments. *Electrochemistry Communications*, 13(4):342–345, April 2011.

[11] H. A. Kiehne, *Batteries Technology Handbook*, 2ed. Expert Verlag, Renningen-Malmsheim, Germany, 2003.

[12] H. Zhao and F. Magouls, "A review on the prediction of building energy consumption," *Renewable and Sustainable Energy Reviews*, vol. 16, no. 6, pp. 3586–3592, August 2012.

[13] F. Katiraei, R. Iravani, N. Hatziargyriou, and A. Dimeas, "Microgrids management," *IEEE Power and Energy Magazine*, vol. 6, no. 3, pp. 54–65, May 2008.

[14] X. Qiu, T. A. Nguyen, M. L. Crow, J. Gugenburger, and A. C. Elmore, "A field validated model of a vanadium redox flow battery for microgrids," *IEEE Transactions on Smart Grid*, 2014.

[15] H. Liao, Q. Wu, and L. Jiang, "Multi-objective optimization by reinforcement learning for power system dispatch and voltage stability," in *Innovative Smart Grid Technologies Conference Europe (ISGT Europe), 2010 IEEE PES*, October 2010, pp. 1–8.

[16] F. Lauri, G. Basso, J. Zhu, R. Roche, V. Hilaire, and A. Koukam, "Managing power flows in microgrids using multi-agent reinforcement learning," *Agent Technologies in Energy Systems (ATES)*, 2013.

VITA

Xin Qiu was born in Shanghai, China. He received his BS degree of electrical engineering in 2007 from Shanghai Jiaotong University and worked as a design engineer in Cooper Power Systems in Shanghai from 2007 to 2009. In December 2014, he received his Ph.D. degree in Electrical Engineering from the Department of Electrical and Computer Engineering, Missouri University of Science and Technology (Missouri S&T), Rolla, MO, USA.